NASA Contractor Report 165772

FINAL REPORT

AN INFLUENCE COEFFICIENT METHOD FOR THE

APPLICATION OF THE MODAL TECHNIQUE TO

WING FLUTTER SUPPRESSION OF THE DAST ARW-1 WING

Samuel Pines
Judy McConnell

ANALYTICAL MECHANICS ASSOCIATES, INC.
Hampton, VA 23666

NASA

National Aeronautics and
Space Administration

Langley Research Center
Hampton, Virginia 23665

SUMMARY

This report describes the methods used to compute the mass, structural stiffness and aerodynamic forces in the form of influence coefficient matrices as applied to a flutter analysis of the DAST ARW-1 wing. The DAST wing was chosen since wind tunnel flutter test data and zero speed vibration data of the modes and frequencies exist and are available for comparison.

The report also contains a derivation of the equations of motion that can be used to apply the modal method for flutter suppression. A comparison of the open loop flutter prediction with both wind tunnel data and other analytical methods is presented.

INTRODUCTION

Real time, feedback control for flutter suppression is under serious study and consideration for aircraft (Refs. 1,2,3,4). The modal method (Refs. 5,6) is well suited for application in flutter suppression since the onset of flutter may be adequately described as a linear system instability (Ref. 7). Previous analyses of the problem have employed generalized coordinates, based on zero airspeed vibration modes or other fixed wing deformation shapes, from which generalized aerodynamic forces have been computed (Refs. 1,2,4). The contribution of this report is that physical coordinates of bending and torsion of the wing structure are directly employed, and that constant influence coefficient matrices are used to describe the structural, inertial and aerodynamic forces over a wide range of Mach numbers and airspeed. The aerodynamic influence coefficients were obtained through a modification of the SOUSSA digital program (Refs. 8,9) generated with the assistance of Prof. L. Morino of Boston University, Dr. E. C. Yates and H. Cunningham of NASA/LaRC. In contrast, the aerodynamic coefficients used in Ref. 1,4 were obtained using a doublet lattice method (Ref. 10). The method of Pade' approximants (Refs. 7,11,12,13) was applied to derive the aerodynamic influence coefficients in the real time domain. The structural influence coefficients were obtained through the use of the SPAR computer program at NASA/LaRC. Finally, the structural and geometric data of the DAST ARW-1 Wing, at 111 grid points, was supplied by Mr. R. Doggett of NASA/LaRC.

I. Description of the Wing Flutter Model

The DAST ARW-1 wing was designed at the Langley Research Center as a swept back, cantilevered wind tunnel flutter model of a prototype, remotely-piloted, drone aircraft used to study active control concepts including flutter suppression. The data used in this report for determining the inertial and structural characteristics of the wing, as well as the results of vibration and wind tunnel flutter tests, was furnished by Mr. R. Doggett of NASA/LaRC.

The geometric planform and dimensions of the wing are shown in Fig. 1. The leading edge has a sweep back angle of 44.32°. The wing has a taper ratio of .392 and an aspect ratio of 6.4. The airfoil is a NACA 65A10 section. The main structural beam is a single tapered aluminum bar construction with a cruciform cross section (see Fig. 2). The dimensions of the spar cross section at various locations along the length are shown in Table 1. The measured stiffness distribution is shown in Fig. 3 in terms of the bending and torsional stiffness, EI and GJ curves.

The wing is divided into eight pod sections by means of seven ribs oriented in the stream direction (see Fig. 4). Each section contains concentrated masses rigidly connected to the main beam to provide realistic mass offsets with respect to the local elastic axis. Each section is covered with balsa inserts and the aerodynamic shape is maintained by a precured fiberglass cover.

A control surface is provided along the trailing edge, equipped with an electro-hydraulic servo-actuator. The surface hinge line is located at 80% of the local streamwise chord. The reaction torques of the actuator are constrained by a link to the main structural beam in the control surface pod section.

A Cartesian coordinate system is used in the analysis. The origin of the system is at the intersection of the wing root chord and the wing leading edge. The x-axis is positive forward in the streamwise direction. The z-axis is positive down, and the y-axis forms a right hand system. (See Fig. 4). The structural axis of the beam defines the y' coordinate, rotated at an angle of 40.7° with respect to the y axis. The origin of the x', y', z' system is at (-.372364, 0., 0.).

Thus

$$\begin{Bmatrix} x' \\ y' \\ z' \end{Bmatrix} = \begin{pmatrix} \cos\theta & \sin\theta & 0 \\ -\sin\theta & \cos\theta & 0 \\ 0 & 0 & 1 \end{pmatrix} \begin{Bmatrix} x + .372364 \\ y \\ z \end{Bmatrix} \qquad (1)$$

where $\theta = 40.7^\circ$.

The dynamical coordinates are located along the y' axis (see Fig. 5). These consist of seven vertical deflections, $h\,(y'_i)$ ($i = 1,7$), seven rotations in the air stream direction, $\alpha\,(y'_i)$ ($i = 1,7$), and a single rotation about the control surface hinge line, δ . Thus the dynamical coordinates form a 15 x 1 vector given by

$$\{w\} = \begin{Bmatrix} h_1 \\ h_2 \\ \cdot \\ \cdot \\ h_7 \\ \alpha_1 \\ \alpha_2 \\ \cdot \\ \cdot \\ \alpha_7 \\ \delta \end{Bmatrix} \qquad (2)$$

The equations of motion will be generated in terms of the forces and moments affecting these 15 degrees-of-freedom. The center line, or root section, is constrained to maintain zero deflection in the vertical direction and in stream-wise rotation. Thus $h\,(0) = \bar{\alpha}\,(0) = 0$.

II. Structural Influence Coefficients

The structural influence coefficients were computed utilizing the SPAR computer program at the LRC computer facility. The SPAR program requires that the wing be decomposed into a series of grid points. At each point, six degrees-of-freedom are permitted. There are three translations along, and three rotations about each of the three axes. A finite element method is employed to compute the linear relationships between the deformations of the grid points with respect to one another and the resulting forces and moments resisting these deformations. For the DAST wing, a grid decomposition of 111 was used, resulting in 666 degrees-of-freedom. (See Figure 6). Of these, points 103 through 109 correspond to the concentrated masses which undergo rigid motions without relative structural deformations. Point 111 is the control surface linkage constraint for rotation about the hinge line.

To produce the structural influence coefficients for the 15 degrees-of-freedom defined by the dynamical coordinate vector, w , we constrained 7 points in 2 degrees-of-freedom (vertical deflection and rotation in the flight direction) and the 15th degree-of-freedom to be a pure rotation about the hinge line. All other degrees-of-freedom in the original SPAR deformation are left unconstrained except for the root section grid points (97, 100 and 102) which are constrained in three directions. (See Figure 7). The SPAR program solves a static equilibrium problem for which one coordinate of w is set equal to unity, and the other twenty-three are constrained to be zero. The forces and moments at the 24 locations are computed by solving a set of 24 equations of equilibrium. Thus, we have

$$
\left\{ \begin{array}{c} F_{\ell} \\ M_{\ell} \\ F_{0,\ell} \\ M_{0,\ell} \end{array} \right\}_{24 \times 1}
=
\left[\begin{array}{c|c} K_{15 \times 15} & k_{i,16} \cdot k_{i,24} \\ \hline k_{16,j} & \\ k_{24,j} & \end{array} \right]_{24 \times 24}
\left\{ \begin{array}{c} 0 \\ \vdots \\ 0 \\ 1 \\ 0 \\ \vdots \\ 0 \end{array} \right\}_{24 \times 1}
\tag{3}
$$

where the ℓth element of w, w_ℓ, $= 1$ and all other elements, including $h(0)$ and $\alpha(0)$, are set equal to zero. The forces, $F_{0,\ell}$, and the moments, $M_{0,\ell}$, are the reactions at the root section required to hold the root section undeformed.

The elements of the ℓth column of the influence coefficient matrix (K) are given by

$$\left\{ \bar{k}_{i,\ell} \right\}_{15\times1} = \left\{ \begin{array}{c} F_\ell \\ M_\ell \end{array} \right\}_{15\times1} \tag{3a}$$

The deflections at the remaining 642 grid points are left unconstrained. The matrix of influence coefficients is given in Table 2. The units are in Newtons per meter of deflection, Newtons per radian, Newton-meters per meter of deflection and Newton-meters per radian arranged as follows:

$$\left(\begin{array}{c|c} \text{Newtons/meter (7x7)} & \text{Newtons/rad (7x8)} \\ \hline \text{Newton-meter/meter} & \text{Newton-meter/rad} \\ (8x7) & (8x8) \end{array} \right) \tag{4}$$

III. Mass Data

The SPAR program carries out a vibration analysis of the DAST wing by solving an eigenvalue problem utilizing the input mass and stiffness data at the 111 grid points. Of the 666 degrees-of-freedom, 18 at the root section (grid points 97, 100 and 102) are constrained to be fixed, and 42 correspond to the 7 rigidly attached concentrated masses (103 through 109). For the purposes of this study, the number of degrees-of-freedom has been reduced to 15 plus 9 fixed, root degrees-of-freedom. In order to produce a simulation in which the significant vibration modes are well represented, it is necessary to compute a set of lumped masses at the c.g.'s of the seven sections, which, together with the rigid concentrated masses and the 15x15 influence coefficient matrix, will reproduce the significant low-order vibration modes.

To accomplish this, the distributed beam and plate masses have been summed in 7 sections and are listed in Table 3. The concentrated masses are listed in Table 4.

The combined masses acting at each of the sections' c.g.'s form the diagonal elements of the mass matrix (in units of kilograms in the mks system). The off-diagonal elements are obtained from the static unbalance due to the offset of the concentrated masses from the coordinate c.g.'s (see Table 4). M, the desired mass matrix used in the equations of motion, is listed in Table 5.

IV. Frequencies and Modes

To ensure that the SPAR representation of the DAST cantilevered wing is a valid simulation of the wind tunnel model, a comparison of the first four computed and measured vibration modes was carried out using the full 111 grid-point model. Figure 8 contains the results of the vibration test furnished by R. Doggett of NASA/LaRC. Figures (9a), (9b), (9c), and (9d) are plots of the same modes with the SPAR program using all of the 111 grid points. The comparison is seen to be good. Figures 10 and 11 contain the next two highest modes obtained by the SPAR program for which no vibration data is available.

Finally, in order to test the validity of the reduced 15 degrees-of-freedom model, an eigenvalue analysis using the mass, M , and influence coefficient, K , matrices was carried out. The results of the analysis are shown in Figures (12a), (12b), (12c), and (12d) for the first four modes. The agreement is seen to be good. The 15 degrees-of-freedom eigenvalues are shown in Table 6 together with the vibration test frequencies and those frequencies obtained with the full 666 degrees-of-freedom.

V. Equations of Motion

The forces acting on the wing in the air speed region containing the flutter speed are assumed to consist of the following:

(a) inertia

(b) unsteady aerodynamic forces

(c) structural restraint to wing deformation

(d) random aerodynamic forces due to wind gusts

(e) a stabilizing feedback torque acting on the control response

(f) aerodynamic forces due to the control surface deflection

To simulate these forces, assuming small deflections, we require the dynamic coordinate vector, w , its first and second time derivatives, $\dot{w}$ and $\ddot{w}$, the unsteady lift and moment vector, $x_{p_{15 \times 1}}$, its time derivative vector, $\dot{x}_p$, three scalar gust variables (x_{1D}, x_{2D} and w_g), and the scalar control torque, u_A.

The equations of motion are given by

$$
\begin{pmatrix} I & 0 & 0 \\ 0 & M & 0 \\ 0 & -H_3 & I \end{pmatrix}_{45 \times 45} \frac{d}{dt} \begin{Bmatrix} w \\ \dot{w} \\ x_p \end{Bmatrix}_{45 \times 1} = \begin{pmatrix} 0 & I & 0 \\ -K & -D_w & qI \\ H_1 & H_2 & F_p \end{pmatrix}_{45 \times 45} \begin{Bmatrix} w \\ \dot{w} \\ x_p \end{Bmatrix}_{45 \times 1} \tag{6}
$$

$$
+ \begin{Bmatrix} 0 \\ B \\ 0 \end{Bmatrix}_{45 \times 1} u_A + \begin{Bmatrix} 0 \\ \gamma \\ 0 \end{Bmatrix} (.13 \frac{v}{c^2} q\, x_{1D} + .565 \frac{q}{c} x_{2D})
$$

and

$$
\frac{d}{dt} \begin{Bmatrix} x_{1D} \\ x_{2D} \end{Bmatrix}_{2 \times 1} = \begin{pmatrix} 0 & g_{12D} \\ (\frac{v}{c})^2 g_{21D} & \frac{v}{c} g_{22D} \end{pmatrix}_{2 \times 2} \begin{Bmatrix} x_{1D} \\ x_{2D} \end{Bmatrix}_{2 \times 1} + \begin{Bmatrix} 0 \\ \tilde{w}_g \end{Bmatrix}_{2 \times 1} \tag{6a}
$$

where

$$I \quad = \quad \text{15x15 identity matrix}$$

D_w = 15x15 structural damping matrix (see Table 8)

M = 15x15 matrix of masses

K = 15x15 structural influence coefficient matrix from the SPAR program

H_1 , H_2 , H_3 are constant 15x15 aerodynamic influence coefficient matrices obtained by Pade Approximates from the SOUSSA output. (See Table 7b, c, d)

B = 15x1 vector of 0's except at the points of application of the feedback torque, u_A , where $b_{13} = -1$ and $b_{15} = 1$.

$$\{ \gamma \}_{15x1} = (H_0)_{15x15} \begin{Bmatrix} 0 \\ 0 \\ 0 \\ 0 \\ 0 \\ 0 \\ 0 \\ 1 \\ 1 \\ 1 \\ 1 \\ 1 \\ 1 \\ 1 \\ 1 \end{Bmatrix} \qquad (6b)$$

$$15x1$$

H_0 = 15x15 steady state lift and moment distribution matrix obtained from SOUSSA (See Table 7a)

c = half the mean aerodynamic chord (.2524379 m)

q = $\frac{1}{2} \rho v^2$ (dynamic pressure)

v = air speed

ρ = density

b = reference length used in the SOUSSA program (b = 1 inch)

$\tilde{w}_g$ = scalar random wind gust

To facilitate the transformation to modal coordinates, the matrix containing M and H_3 may be inverted. The, Equation 6 becomes

$$\frac{d}{dt} \left\{ \begin{array}{c} w \\ \dot{w} \\ x_p \end{array} \right\} = \left(\begin{array}{ccc} 0 & I & 0 \\ -M^{-1}K & -M^{-1}D_w & q\,M^{-1} \\ H_1-H_3\,M^{-1}K & H_2-H_3\,M^{-1}D_w & F_p+q\,H_3\,M^{-1} \end{array} \right) \left\{ \begin{array}{c} w \\ \dot{w} \\ x_p \end{array} \right\} \quad (6c)$$

$$+ \left\{ \begin{array}{c} 0 \\ M^{-1}B \\ H_3\,M^{-1}B \end{array} \right\} u_A + \left\{ \begin{array}{c} 0 \\ M^{-1}\gamma \\ H_3\,M^{-1}\gamma \end{array} \right\} (.13\,\frac{v}{c^2}\,q\,x_{1D} + .565\,\frac{q}{c}\,x_{2D})$$

To obtain a good model for the structural damping matrix, D_w, we make use of the approximation that the structure provides approximately .5% of critical damping.

Thus, let

$$M^{-1}K = U(\omega_i^2)\,U^{-1} \quad (6d)$$

where the matrix U is the matrix of eigenvectors of $M^{-1}K$ and ω_i^2 is the diagonal matrix of the eigenvalues. We have as a good approximation of D_w,

$$D_w = .01\,(M)\,U(\omega_i)\,U^{-1} \quad (6e)$$

where ω_i is a diagonal matrix of the square roots of the eigenvalues of Eq. (6d). The matrix D_w is given in Table 8.

VI. The SOUSSA Program and the Padé Approximants

The SOUSSA digital program (Refs. 8, 9) computes generalized aerodynamic forces for a wing of given planform executing sinusoidal oscillations in a fixed wing deflection mode shape. The generalized forces are computed at a given Mach number, m , for a given non-dimension frequency, $k = \dfrac{\omega b}{v}$, a characteristic length, b , and a non-dimensional time variable $T = \dfrac{v}{b} t$. The generalized forces are given in terms of the force per unit dynamic pressure, q. Thus we have

$$\left\{ \frac{\bar{L}(j\omega)}{q} \right\} = \left(Q_R(m,k) + j\, Q_I(m,k) \right) \left\{ \bar{W}(j\omega) \right\} \tag{7}$$

where $j = \sqrt{-1}$ and $\bar{W}(j\omega)$ is the non-dimensional deflection mode shape oscillating at the sinusoidal frequency, ω.

In the application we seek in this study, we desire to obtain the aerodynamic forces in influence coefficient form. To obtain this, a pre-processor was developed by Prof. L. Morino to generate 17 unit impulse function modes for $\bar{W}(j\omega)$ corresponding to each of the 15 coordinates of our dynamical state w , plus the root section degrees-of-freedom, h(0) and $\alpha(0)$. Thus, for the ith unit impulse function mode we have unit deflection for the ith element and zeroes for the other fourteen elements.

We obtain the ith column of the desired aerodynamic influence coefficient matrix from Eq. (7)

$$\left\{ \frac{\bar{L}(j\omega)}{q} \right\}_i = \left\{ q_{Ri}(m,k) + j\, q_{Ii}(m,k) \right\} \tag{8}$$

The SOUSSA coordinate system is positive deflection upward, and a positive angle of attack is trailing edge upward. Consequently, we have

$$\left\{ \bar{W}(j\omega) \right\} = -\left\{ \begin{array}{c} \dfrac{\bar{h}(j\omega)}{b} \\[6pt] \bar{\alpha}(j\omega) \\[6pt] \bar{\delta}(j\omega) \end{array} \right\} \tag{9a}$$

By choosing the characteristic length b to be unity, we have

$$\left\{ \bar{W}(j\omega) \right\} = - \left\{ \bar{w}(j\omega) \right\} \tag{9b}$$

The SOUSSA generalized force is positive upward, and the generalized moment is positive for a positive (upward) force acting aft of the rotation axis. Thus, we have

$$\left\{ \bar{x}_p(j\omega) \right\} = - \left\{ \frac{\bar{L}(j\omega)}{q} \right\} \tag{9c}$$

Finally, we have from the relation between time, t , and T

$$\frac{d}{dt} \left\{ \bar{w}(j\omega) \right\} = - \frac{v}{b} \frac{d}{dT} \left\{ \bar{W}(j\omega) \right\} \tag{10}$$

and

$$\frac{d^2}{dt^2} \left\{ \bar{w}(j\omega) \right\} = - \left(\frac{v}{b} \right)^2 \frac{d^2}{dT^2} \left\{ \bar{W}(j\omega) \right\}$$

The resulting unsteady lift, $\bar{x}_p(j\omega)$, for the non-dimensional sinusoidal $\bar{W}(j\omega)$ vector is given by the Laplace transform of the last fifteen (15) rows of the matrix Eq. (6),

$$\left\{ \bar{x}_p(j\omega) \right\} = - \left(j \frac{v}{b} k \, I - F_p \right)^{-1} \left(H_1 + j \frac{v}{b} k H_2 - \left(\frac{v}{b} k \right)^2 H_3 \right) \left\{ \bar{W}(j\omega) \right\} \tag{11}$$

and from Eq.'s (7) and (9c) we have

$$\left\{ \bar{x}_p(j\omega) \right\} = - \left(Q_R(m,k) + j \, Q_I(m,k) \right) \left\{ \bar{W}(j\omega) \right\} \tag{12}$$

It then follows that

$$\left(j \frac{v}{b} k \, I - F_p \right)^{-1} \left(H_1 + j \frac{v}{b} k H_2 - \left(\frac{v}{b} k \right)^2 H_3 \right) = Q_R(m,k) + j \, Q_I(m,k) \tag{13}$$

To determine the desired constant matrices, independent of time and frequency, we have recourse to the Padé Approximants of Ref.'s 7,11,12,13. In what follows below, we lean heavily on the work of Edwards in Ref. 12.

Since there are four (4) unknown matrices to be determined, we can, at most, satisfy only four (4) conditions. For the first condition, we choose to satisfy Eq. (13) at $k = 0$. We have

$$H_1 = -F_p Q_R (m, 0) \tag{14}$$

For the second condition, we choose to determine H_3 from the real part of Eq. (13) giving

$$H_3 = (\frac{b}{vk})^2 F_p \Big(Q_R(m,k) - Q_R(m,0) \Big) + (\frac{b}{vk}) Q_I (m,k) \tag{15}$$

As k increases beyond bound, we have the piston theory limit (Ref. 14)

$$H_3 = \frac{b}{v} Q_{piston} (m) \qquad (b = 1.) \tag{16}$$

The nonzero elements of Q_{piston}, q_{ij}, are given by $(i = 1,7)$

$$q_{i,1} = -\frac{4\alpha}{m} \left(\frac{C_i^2 - C_{i+1}^2}{2} \right)$$

$$q_{i,i+7} = -\frac{4\alpha}{m} \left(\frac{C_i^3 - C_{i+1}^3}{3} \right) \left(\frac{1 - 2x_o}{2} \right)$$

$$q_{i+7,i} = q_{i,i+7}$$

$$q_{i+7,q_{i+7}} = -\frac{4\alpha}{m} \left(\frac{C_i^4 - C_{i+1}^4}{4} \right) (1 - 3x_o + 3x_o^2) \tag{16a}$$

$$q_{6,15} = -\frac{4\alpha}{m} \left(\frac{C_6^3 - C_7^3}{3} \right) (1 - x_1)(1 + x_1 - 2x_o)$$

-13-

$$q_{13,15} = -\frac{4\alpha}{m}\left(\frac{C_6^4 - C_7^4}{4}\right)\left(1 - \frac{x_1^3}{3} - \frac{1 - x_1^2}{2}(x_o + x_1) + x_o x_1(1 - x_1)\right)$$

$$q_{15,6} = q_{6,15}$$

$$q_{15,13} = q_{13,15}$$

$$q_{15,15} = -\frac{4\alpha}{m}\frac{C_6^4 - C_7^4}{4}\frac{1 - x_1^3}{3} \tag{16a}$$

where

$$\alpha = \frac{1.9431}{.8764016 - .3431794}$$

C_i = wing chord in stream direction at the start of the ith section

x_o = elastic axis in % of chord $\qquad$ (.4231)

x_1 = hinge line axis in % of chord $\qquad$ (.80)

The values of the C_i are

i	C_i (meters)
1	.8353
2	.7534
3	.6784
4	.6087
5	.5390
6	.4697
7	.4205
8	.3432

We choose as our third condition to match the imaginary part of Eq. (13) to the SOUSSA output for the flutter-reduced frequency, k_f. Thus we have

$$H_2 = Q_R(m,k_f) - \frac{F_p \, Q_I \, (m,k_f)}{k_f} \left(\frac{V}{b} \right) \tag{17}$$

Finally, we choose for F_p a diagonal matrix to provide stable poles for the homogenous differential equation for the x_p variable. We choose for F_p

$$F_p = - \frac{\sigma \, v}{b_{ref}} \begin{bmatrix} \dfrac{b_{ref}}{b_1} & & & & & & & 0 \\ & \ddots & & & & & & \\ & & -\dfrac{b_{ref}}{b_7} & & & & & \\ & & & \dfrac{b_{ref}}{b_1} & & & & \\ & & & & \ddots & & & \\ & & & & & \dfrac{b_{ref}}{b_7} & & \\ 0 & & & & & & \dfrac{b_{ref}}{b_6} \end{bmatrix} \tag{18}$$

when b_1, $b_2 \ldots b_7$ are the local semi-chords of the seven y_i' stations at which the 15 coordinates are defined. The semi-chord used for the control surface (i = 15) is the semi-chord corresponding to the sixth (6) wing panel.

In order to determine the best value of σ, a one dimensional search was undertaken to determine the open loop flutter analysis for the homogenous matrix differential equation (Eq. (6c)) at a dynamic pressure of q = 5.36 kPa, a mach number of .897, and a v of 136 meters/sec. The best value of σ proved to be $\sigma = +2.249$.

VII. Open Loop Flutter Analysis

The results of the open loop flutter analysis of the DAST wing using the influence coefficient method was carried out by determining the eigenvalues of the homogenous part of the differential matrix equation (6c).

$$
\frac{d}{dt} \left\{ \begin{array}{c} w \\ \dot{w} \\ x_p \end{array} \right\} = \left(\begin{array}{ccc} 0 & I & 0 \\ -M^{-1}K & -M^{-1}D_w & q\,M^{-1} \\ H_1 - H_3 M^{-1}K & H_2 - H_3 M^{-1}D_w & F_p + q H_3 M^{-1} \end{array} \right) \left\{ \begin{array}{c} w \\ \dot{w} \\ x_p \end{array} \right\} \tag{19}
$$

for different values of the dynamic pressure, q, for a fixed Mach number (m = .897) and fixed airspeed (v = 136 m/sec).

The results of the study, shown in Figure 13, are to be compared to a similar plot taken from Ref. 1 shown in Figure 14. In order to illustrate a more detailed comparison of the pertinent flutter modes, we have Fig. 15 which is a plot of the frequency and damping versus dynamic pressure for the open loop system.

The wind tunnel results as obtained from R. Doggett were

$$
\begin{array}{lll}
m & = & .897 \\
q & = & 5.36 \text{ kPa} \\
v & = & 136 \text{ m/sec} \\
\omega & = & 8.0 \text{ Hz}
\end{array} \tag{20}
$$

The comparison is shown to be good with both the wind tunnel data and the analytical prediction of Abel (Ref. 1).

REFERENCES

1. Abel, I., "An Analytic Technique for Predicting the Characteristics of a Flexible Wing Equipped With an Active Flutter Suppresion System and Compared With Wind Tunnel Data," NASA TN 1367, 1979.

2. Gangsaas, D., and Ly, U., "Application of a Modified Linear Quadratic Gaussion Design to Active Control of a Transport Airplane," A. I. A. A. Conference on Guidance and Control, Aug. 6-8, 1979, Boulder, Col.

3. Nissim, E., and Abel, I., "Development and Application of an Optimization Procedure for Flutter Suppression Using the Aerodynamic Energy Concept," NASA TP 1137, Feb., 1978.

4. Edwards, J. W., Breakwell, J. V., Bryson, A. E., "Active Flutter Control Using Generalized Unsteady Aerodynamic Theory," J.G.C., Vol. 1, No. 1, Jan. - Feb., 1978.

5. Creedon, J., "Control of the Optical Surface of a Thin, Deformable Primary Mirror with Application to an Orbitory Astronomical Observatory," Automatica, Vol. 6, pp. 643-660, 1970.

6. Ostroff, A. J., "Evaluation of Control Laws and Actuator Locations for Control Systems Application to Deformable Astronomical Telescope Mirror," NASA TN D-7276, Oct., 1973.

7. Edwards, J. W., "Unsteady Aerodynamic Modeling and Active Aeroelastic Control," NASA - CR - 148019, Feb., 1977.

8. Morino, L., "Steady, Oscillatory and Unsteady Subsonic and Supersonic Aerodynamics - Vol. I, Theoretical Manual," NASA - CR - 159130, Jan., 1980.

9. Scott, A. S., Pruens, R. D., Tseug, K., Morino, L., "Steady, Oscillatory and Unsteady Subsonic and Supersonic Aerodynamics - Vol. II - User's Manual," NASA CR 159131, June 1980.

10. Albano, E., Roddes, W. P., "A Doublet Lattice Method for Calculating Light Distributions on Oscillating Surfaces in Subsonic Flows," A. I. A. A. J., Vol. 7, No. 2, Feb., 1969.

11. Vepa, R., "On the Use of Pade´ Approximants to Represent Unsteady Aerodynamic Loads for Arbitrary Small Motions of Wings," A. I. A. A. 14th Aerospace Science Meeting, Washington, D. C., Jan. 26, 1976.

12. Edwards, J. W., "Applications of Laplace Transform Methods to Airfoil Motion and Stability Calculations," 20th Structural Dynamics and Materials Conference, April 1979, St. Louis, Missouri.

13. Roger, K. L., "Airplane Math Modeling for Active Control Design," AGARD-CP-228, Aug. 1977, pp. 4-1/11.

14. Ashley, H. and Zartarian, G., "Piston Theory - A New Aerodynamic Tool for the Aeroelastician," Journal of the Aerospace Sciences, Dec., 1956, pp. 1109-1118.

15. Jones, R. J., "Operational Treatment of the Nonuniform Lift Theory to Airplane Dynamics," NACA TN 667, 1938.
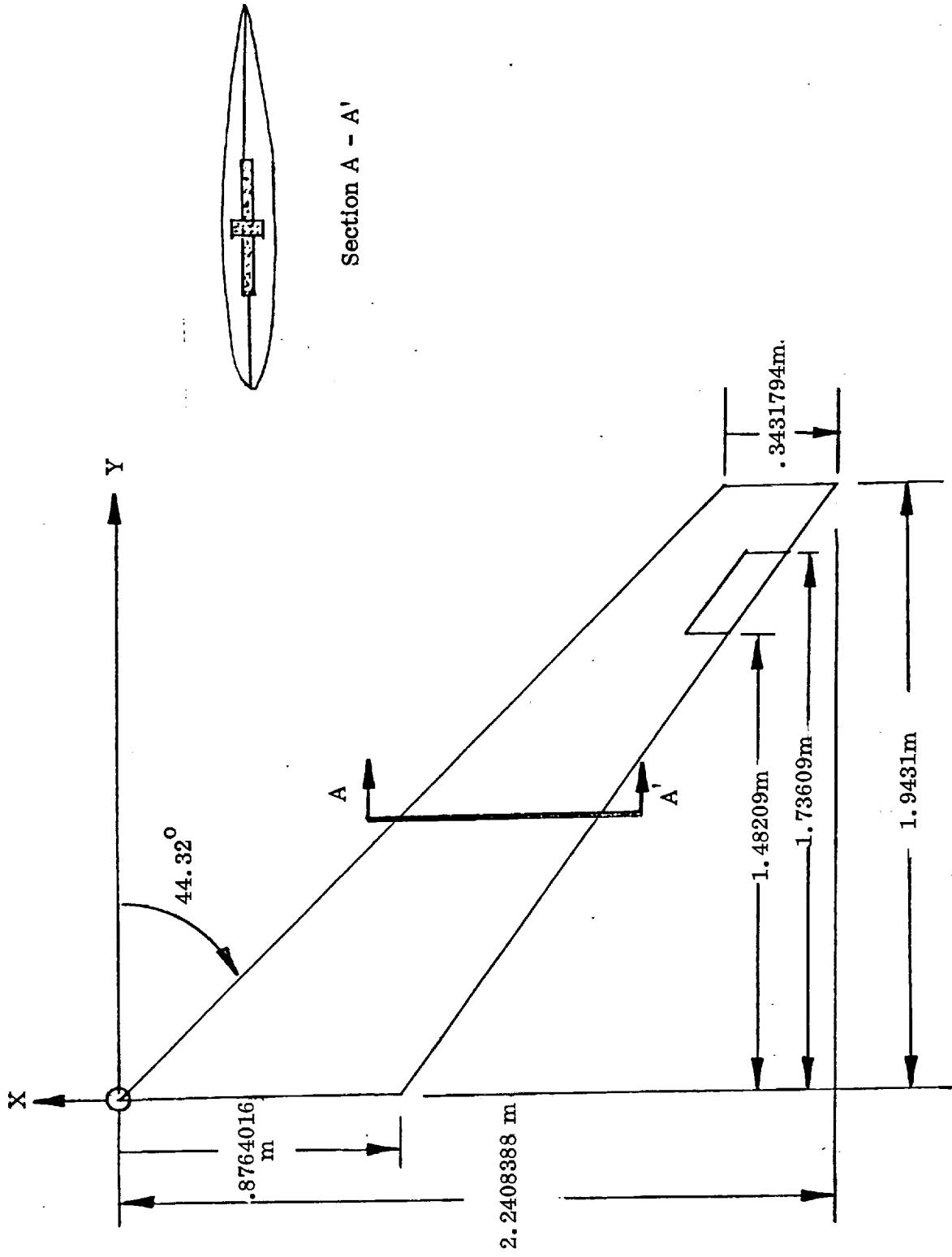
Section A – A'

.3431794m.

.8764016 m

2.2408388 m

1.48209m

1.73609m

1.9431m

44.32°

A

A'

Y

X

Fig. 1 Wing Planform of DAST–ARW1

-19-

TABLE 1 SPAR GEOMETRY DETAILS

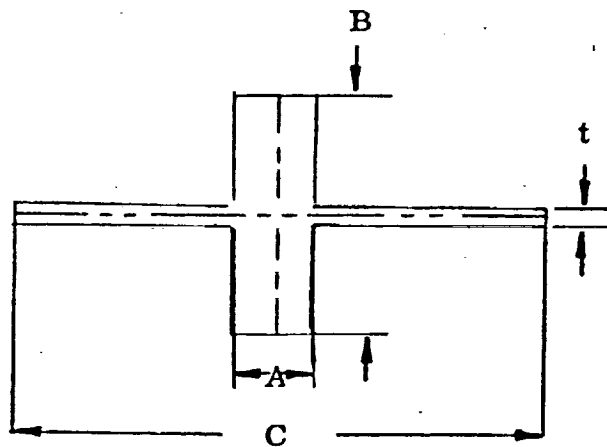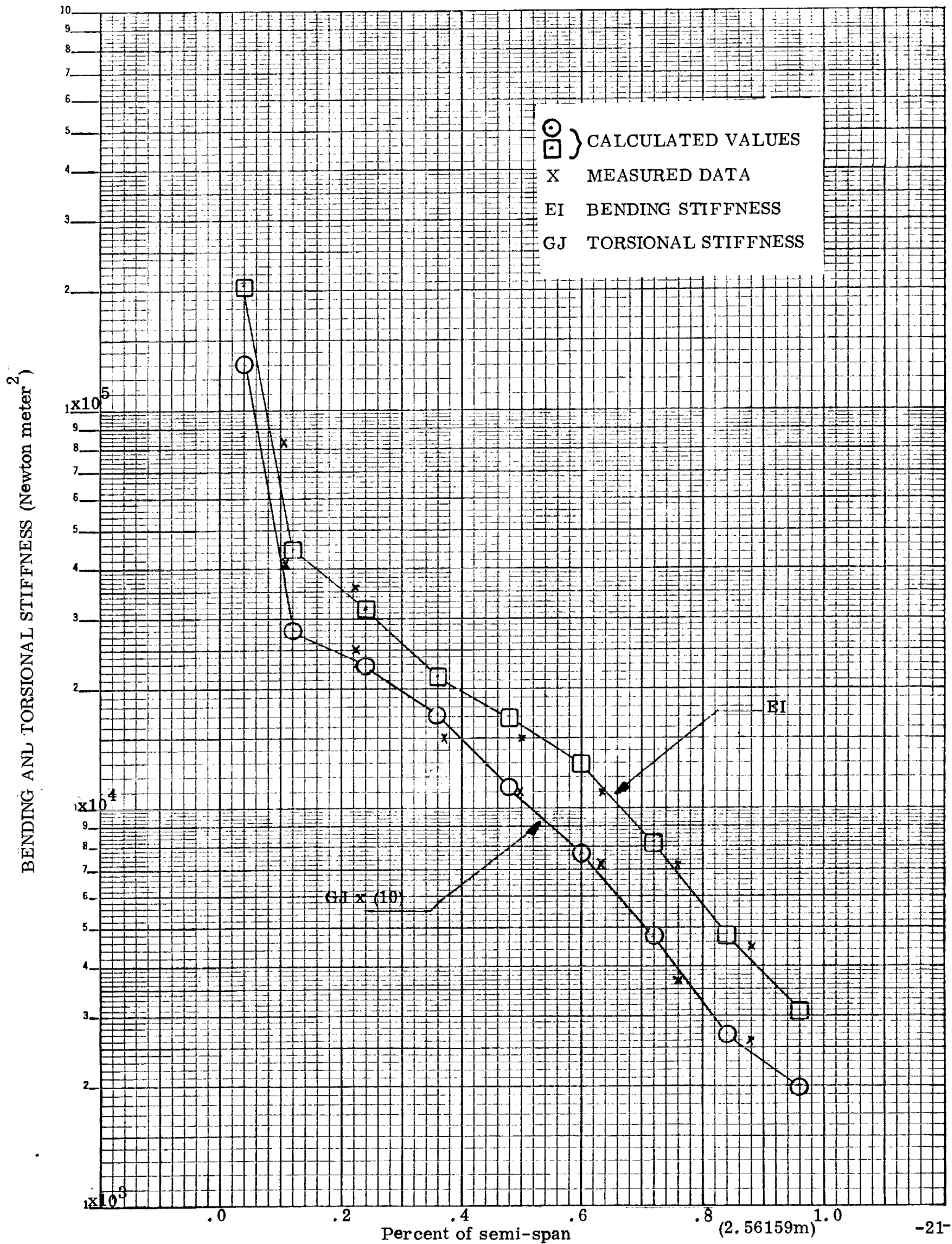| DISTANCE ALONG ELASTIC AXIS METERS	A METERS	B METERS	C METERS	t METERS
0	—	—	—	—
.17145	.0331216	.0722122	.212344	.00508
.393192	.021082	.059436	.201422	.00508
.78232	.01905	.055372	.182372	.00508
1.117346	.017018	.050038	.17526	.00381
1.452118	.015748	.044196	.150368	.00381
1.787398	.014097	.03937	.128524	.00381
2.122424	.013208	.03302	.10287	.00381
2.426208	.010922	.031242	.094488	.00381

Fig. 2   Sketch of spar cross section along elastic axis

Fig. 3 Structural stiffness

Section No.	Y m.
0	0
1	.29972
2	.5969
3	.84582
4	1.1049
5	1.35382
6	1.60782
7	1.83642
8	1.661414

Fig. 4 Coordinate System

STRUCTURAL AXIS

STREAM DIRECTION

X

X'

Y'

Y

h (Y_i')

δ

$\alpha (Y_i')$

X
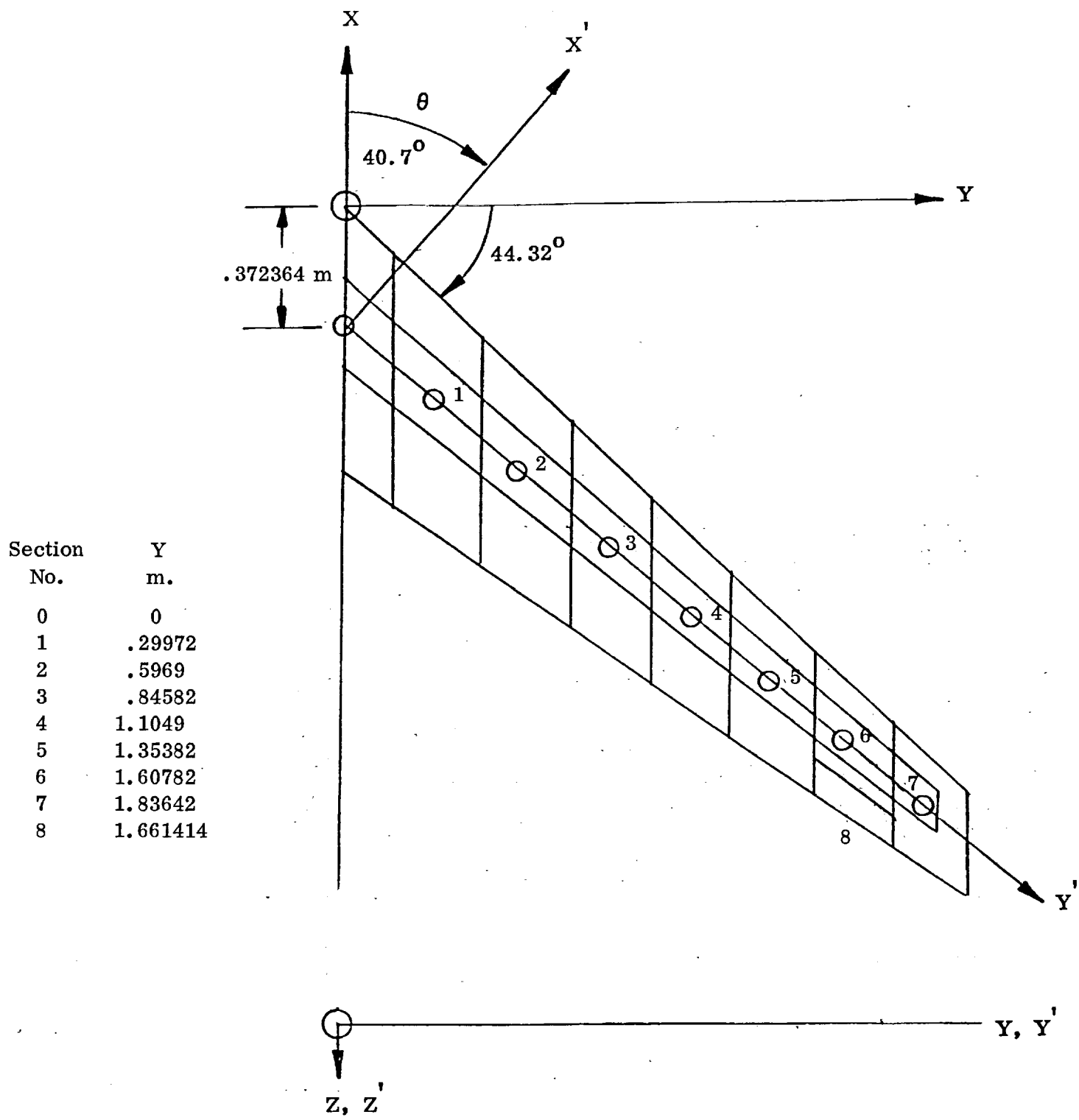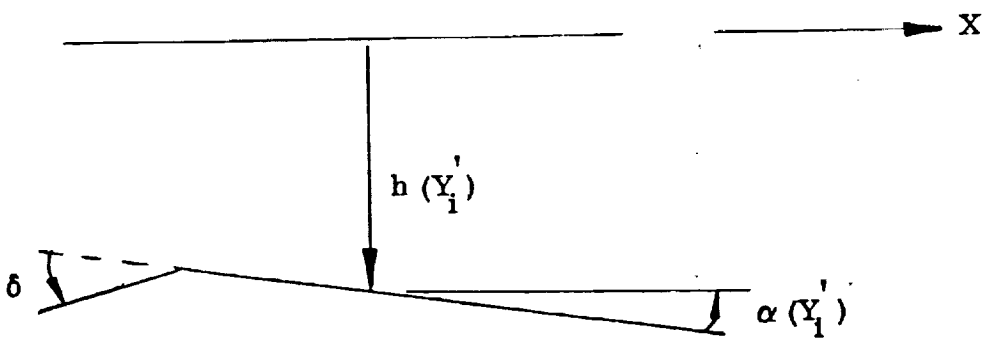
DEGREES OF FREEDOM AT SECTION Y_i'

Fig. 5 Dynamical coordinate system
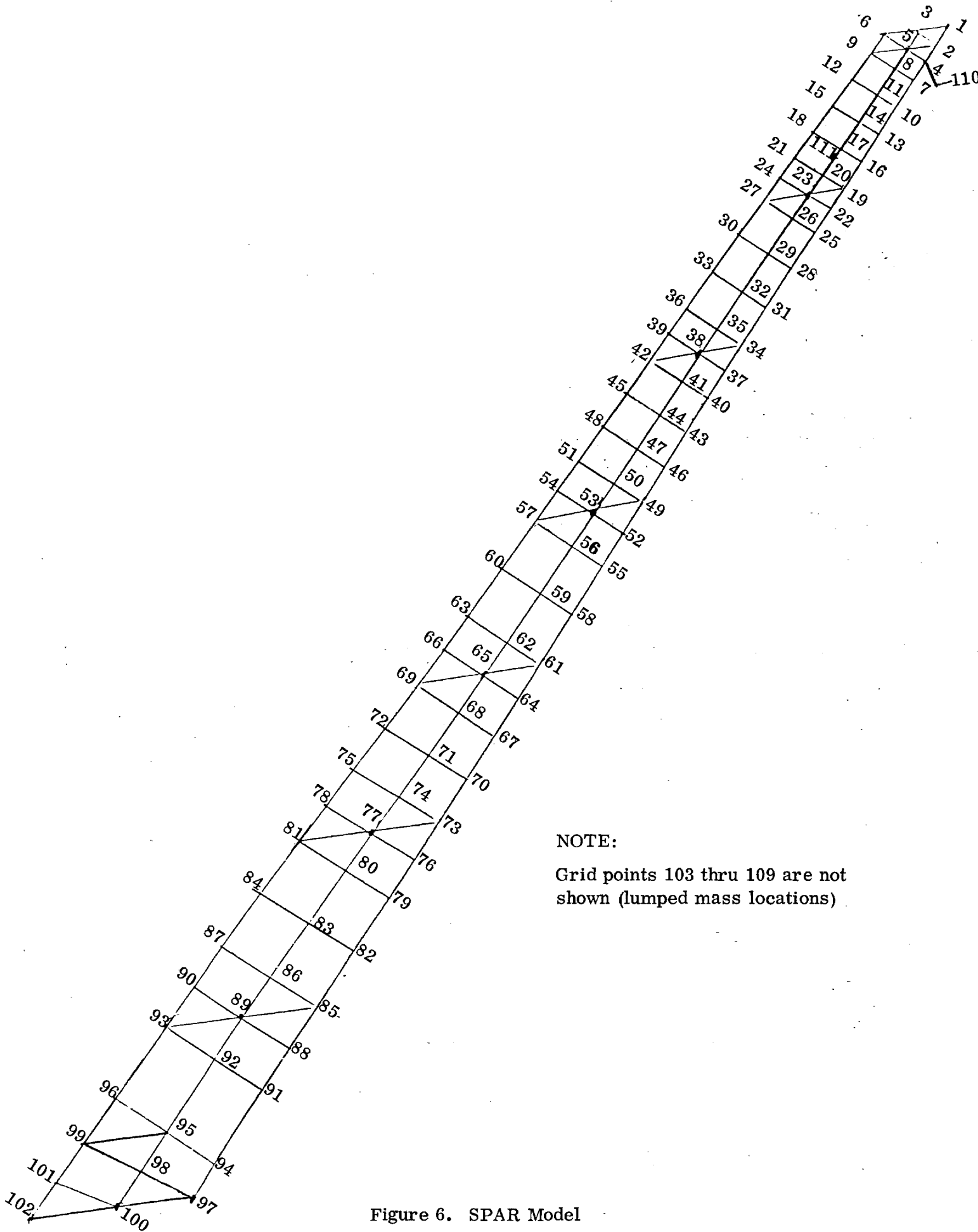
NOTE:

Grid points 103 thru 109 are not
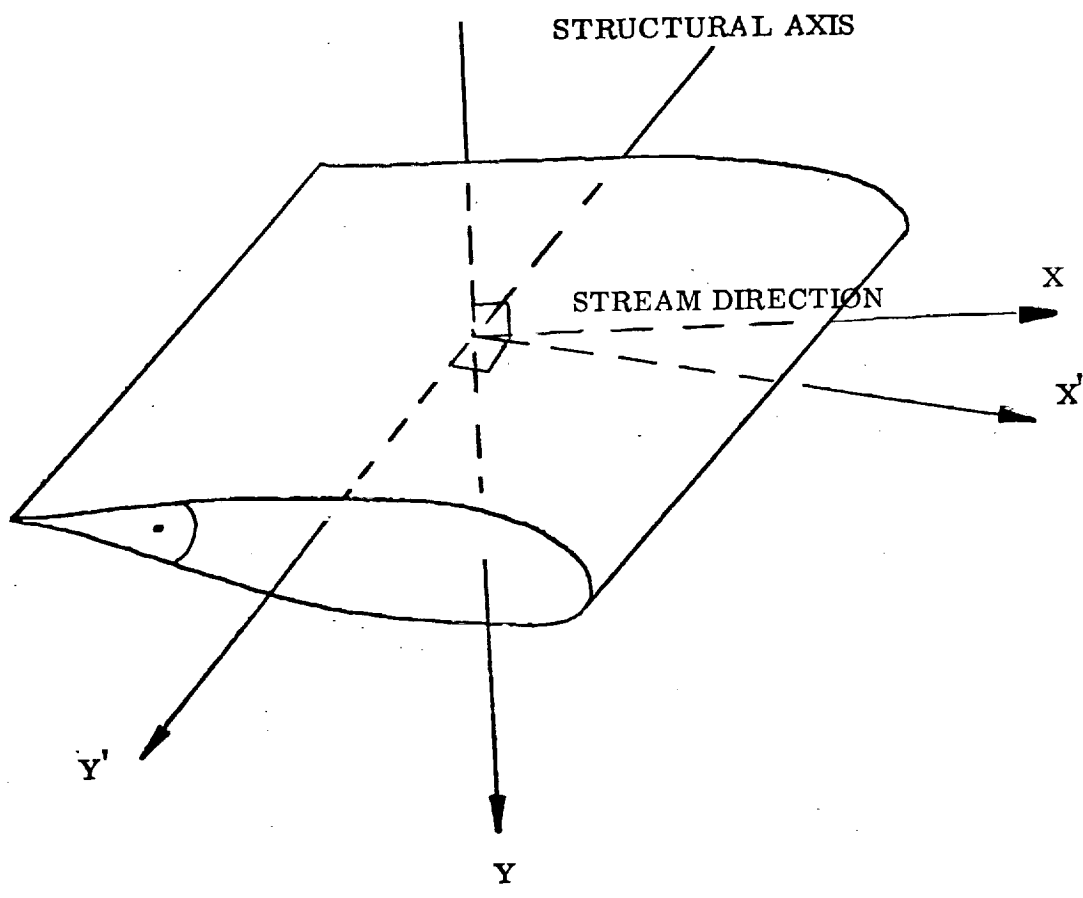shown (lumped mass locations)

Figure 6. SPAR Model

NOTE:

All grid points shown were restrained in DOF 3 and 5. Grid point 100 was also restrained in DOF 4.

Point 111 is the location of the constraint to the actuator torque.

Points 97, 100 and 102 are constrained in DOF 3, 4 and 5.

Figure 7. Grid Points Constrained in Reduced SPAR Model

TABLE 2. Matrix of Influence Coefficients

STRUCTURAL INFLUENCE COEFFICIENT MATRIX

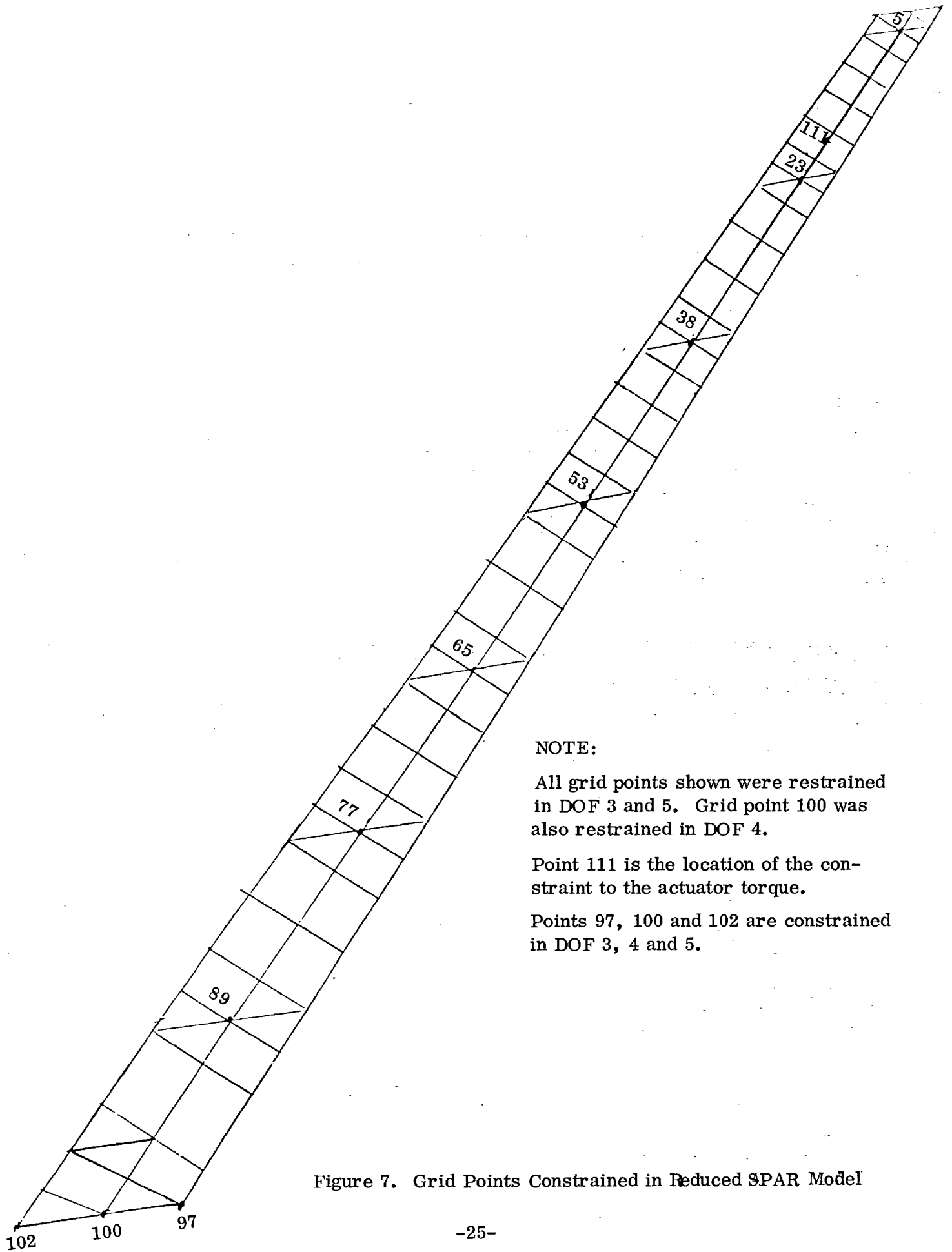| ROW	COL 1	COL 2	COL 3	COL 4	COL 5
1	.22677541630503E+08	-.70437273950212E+07	.23725272946258E+07	-.45362963968582E+06	.91084762822079E+05
2	-.70437273950212E+07	.66060031247437E+07	-.43556373051405E+07	.14240210923139E+07	-.28590646676228E+06
3	.23725272946258E+07	-.43556373051405E+07	.50189196850929E+07	-.29610165058864E+07	.96107680652815E+06
4	-.45362963968582E+06	.14240210923139E+07	-.29610165058864E+07	.32685584920982E+07	-.19638215409079E+07
5	.91084762822079E+05	-.28590646676228E+06	.96107680652815E+06	-.19638215409079E+07	.21367190112963E+07
6	.16839310311815E+05	-.52857009004585E+06	.17766757512218E+06	-.59815586229893E+06	-.11624164510641E+07
7	.22790271159434E+04	.71563987468551E+04	.24054704035576E+05	.80980504848450E+05	.25714118360619E+06
8	.25493803321676E+06	-.14130020564588E+06	.19684572703389E+05	.37508881340771E+04	-.75314708162672E+05
9	.92075518187040E+05	-.10978277632124E+05	.35865855073044E+05	.22395327842872E+05	-.44931530463166E+04
10	.33282972959896E+05	.39630705285079E+05	.95780175064384E+04	.20967252987522E+05	.14092686440699E+05
11	.15316838315552E+05	-.17384828791524E+05	.20228763685711E+05	.58242166768576E+04	-.21338243565405E+05
12	.14706407774851E+04	.46161997922808E+04	.15525392094735E+05	.22592045994910E+05	.84179746918176E+04
13	.48248703157584E+03	-.15144815599304E+04	.50906070291407E+03	-.17114015418765E+05	-.33946766024879E+05
14	.29403225183933E+04	.92929870349816E+04	-.31026640291407E+04	.10443135864550E+05	.33160666024798E+04
15	.13415066803263E+03	-.42108640506018E+03	-.14153916411023E+03	.47649394261416E+04	.15134340037436E+05

ROW	COL 6	COL 7	COL 8	COL 9	COL 10
1	.16839310311815E+05	-.22799027115943E+04	.25493803321676E+06	.92075518187040E+05	.33282972959896E+05
2	-.52857009004585E+06	-.71563987468551E+04	-.14130020564588E+06	-.10978277632124E+05	.39630705285079E+05
3	.17766757512218E+06	.24054704035576E+05	.19684572703389E+05	.35865855073044E+05	.95780175064384E+04
4	.59815586229893E+06	.80980504848450E+05	.37508881340771E+04	.22395327842872E+05	.20967252987522E+05
5	-.11624164510641E+07	.25714118360619E+06	-.75314708162672E+05	-.44931530863816E+04	.14092686440699E+05
6	.10968902939732E+07	-.39724282673302E+06	.13922814180609E+06	-.83067291178232E+04	-.26035997052500E+04
7	-.39724282673302E+06	.20775204024024E+06	-.18851692139226E+06	.11246621048366E+05	.35250563716667E+03
8	.13922814180609E+06	-.18851692139226E+06	.70244588931393E+05	-.13881948805982E+05	-.28450619402627E+03
9	-.13923818804098E+04	.11246621048366E+05	-.13881948805982E+05	.25591945050166E+05	-.11007805700583E+05
10	.83067291178232E+03	.35250563716667E+03	-.28450619402627E+02	-.11007805700583E+05	.18482635504448E+05
11	-.26035997052500E+04	-.14394195997190E+04	.28450619402627E+03	-.27482011762093E+03	-.70618410536622E+04
12	.10635177403673E+05	-.34699415715762E+04	.12160195593817E+04	.72546281972332E+02	-.22310394141981E+03
13	-.58111389053536E+04	.12419799461371E+05	.39895123895626E+01	.23800796556029E+02	.74599645657613E+02
14	.82601117554552E+02	.80457074743352E+04	.24312470951122E+00	.14504438721358E+01	.45461615256867E+01
15	-.22129003919237E+04	.13660862184214E+05	.11092438116594E+01	.66175722777030E+01	-.20741619760258E+02

ROW	COL 11	COL 12	COL 13	COL 14	COL 15
1	.55316838315552E+04	-.14706407774851E+04	.48248703157584E+03	-.29403225183933E+04	-.13415066803263E+03
2	-.17384828791524E+05	.46161997922808E+04	-.15144815599304E+04	.92929870349816E+04	.42108640506018E+03
3	.20228763685711E+05	-.15525392094735E+05	.50906070741424E+04	-.31022640291407E+04	-.14153916411023E+04
4	.58242166768576E+04	.22592045994910E+05	-.17114401541876E+05	.10443819586662E+05	-.47649394261416E+04
5	-.21338243565405E+05	.84179746918176E+04	.33946766024879E+05	-.33160664658782E+04	-.15134340037436E+05
6	.10635177403673E+05	-.58111389053536E+04	.82601117554552E+04	.22129003919237E+04	.22129003919237E+04
7	-.14394195997190E+04	-.34699415715762E+04	.12419799461371E+05	-.80457074743352E+04	-.13660862184214E+05
8	.45739750010416E+02	.12160195593817E+04	.39895123895626E+01	-.24312470951122E+02	-.11092438116594E+01
9	-.27482011762093E+03	.72546281972332E+02	.23800796556029E+02	.14504438721358E+00	.66175722777030E+01
10	-.70618410536622E+04	-.22810394141981E+03	.74599645657613E+02	.45461615256867E+01	-.20741619326025E+02
11	-.12222352353590472E+05	.47593175742298E+04	-.30498356443423E+03	.18563780254636E+02	.84696399319403E+02
12	-.47593175742298E+04	-.82452498018497E+04	.28966417743978E+04	-.44563723805844E+02	-.20315191984413E+03
13	.30498356443423E+03	-.28966417743978E+04	.14334735508200E+05	-.33430934172532E+02	-.85251810141801E+02
14	.18563780254636E+02	-.44563723805844E+04	-.33430934172532E+02	.28029253781354E+04	.20801117136977E+04
15	.84696399319403E+02	-.20315191984413E+03	-.85251810141801E+03	.20801117136977E+04	.81689104722876E+04

-26-

TABLE 3

COMBINED BEAM AND PLATE ELEMENT MASS PROPERTIES

Section No.	Mass (kgm)	$I_{Y'}$ (kgm-m^2)	$I_{X'}$ (kgm-m^2)	$I_{Z'}=I_Z$ (kgm-m^2)	I_X (kgm-m^2)	I_Y (kgm-m^2)
0	7.1088	.0262	.0654	.0913	.0487	.0429
1	2.5310	.0048	.0343	.0382	.0218	.0173
2	1.8328	.0026	.0199	.0220	.0126	.0100
3	1.3659	.0017	.0128	.0142	.0081	.0064
4	1.1339	.0012	.0107	.0116	.0066	.0052
5	.9982	.0010	.0095	.0103	.0059	.0046
6	.7266	.0002	.0058	.0061	.0034	.0026
7	.3341	.0001	.0023	.0024	.0014	.0011

16.0313*

*Compares with 15.8773 kgm calculated by SPAR

TABLE 4

CONCENTRATED MASS PROPERTIES IN X-Y COORDINATE SYSTEM

Section No.	Mass (kgm)	Pitch Inertia I_Y (kgm-m^2)	Yaw Inertia I_Z (kgm-m^2)	Roll Inertia I_X (kgm-m^2)	ΔX** (m)	ΔY** (m)	Pitch Inertia I_Y(grid point) (kgm-m^2)
1	1.6556	.0734	.0801	.0134	-.0051	+.0152	.0734
2	1.0342	.0430	.0443	.0044	+.0147	+.0053	.0432
3	1.1975*	.0333	.0344	.0042	+.0239	+.0036	.0340
4	1.1612*	.0267	.0280	.0034	.0201	.0028	.0272
5	1.0161	.0177	.0192	.0027	.0218	.0041	.0182
6	1.4198	.0200	.0206	-.0047	.0285	.0000	.0211
7***	.6350	.0101	.0127	.0021	-.0521	-.0112	.0118
7***	.5534	.0056	0	.0056	.2070	-.0210	.0293
7***	.4627	0	0	0	0	0	0

9.1355

$$I_{Y(grid\ point)} = I_Y + m\ \Delta X^2$$

* These values were altered to agree with SPAR computer model

** ΔX - Mass offset from grid point in X direction

ΔY - Mass offset from grid point in Y direction

*** These masses were added to cause flutter within the available wind tunnel dynamic pressure.

TABLE 5 MASS MATRIX

MASS MATRIX

ROW	COL 1	COL 2	COL 3	COL 4	COL 5
1	.41866696809275E+01				
2	0.	-.28671590299365E+01			
3	0.	0.	.25632614331610E+01		
4	0.	0.	0.	.22951772741430E+01	
5	0.	0.	0.	0.	.20144139322710E+01
6	0.	0.	0.	0.	0.
7	0.	0.	0.	0.	0.
8	.84106974012800E-02	-.152856587E-01	-.28699480941040E-01	.23302009E-01	-.22293597014880E-01
9	0.	0.	0.	0.	0.
10	0.	0.	0.	0.	0.
11	0.	0.	0.	0.	0.
12	0.	0.	0.	0.	0.
13	0.	0.	0.	0.	0.
14	0.	0.	0.	0.	0.
15	0.	0.	0.	0.	0.

ROW	COL 6	COL 7	COL 8	COL 9	COL 10
1	0.	0.	0.	0.	0.
2	0.	0.	0.	0.	0.
3	0.	0.	0.	0.	0.
4	0.	0.	0.	0.	0.
5	0.	0.	0.	0.	0.
6	.21464070278105E+01	.19853779030280E+01	.84106974012800E-02	-.15235687E-01	-.28699480941040E-01
7	0.	0.	0.	0.	0.
8	0.	0.	0.	0.	0.
9	0.	0.	0.	.90750036069359E-01	0.
10	0.	0.	0.	0.	0.
11	-.40388962483680E-01	-.81494978E-01	0.	.53153972668157E-01	-.40454274515864E-01
12	0.	0.	0.	0.	0.
13	0.	0.	0.	0.	0.
14	0.	0.	0.	0.	0.
15	0.	0.	0.	0.	0.

ROW	COL 11	COL 12	COL 13	COL 14	COL 15
1	0.	0.	0.	0.	0.
2	0.	0.	0.	0.	0.
3	0.	0.	0.	0.	0.
4	-.23302009E-01	-.22293597014880E-01	0.	0.	0.
5	0.	0.	0.	0.	0.
6	0.	0.	0.	0.	0.
7	0.	0.	0.	0.	0.
8	0.	0.	0.	0.	0.
9	0.	0.	0.	0.	0.
10	0.	0.	0.	0.	0.
11	0.	0.	0.	0.	0.
12	.32363656880832E-01	-.22762138321515E-01	-.40388962483680E-01	-.81494978E-01	.42146030255930E-01
13	0.	0.	-.23737502454823E-01	0.	0.
14	0.	0.	0.	0.	0.
15	0.	0.	0.	0.	.26229428052350E-03

MODE 1. - 5.22 hertz

MODE 2. - 19.44 hertz
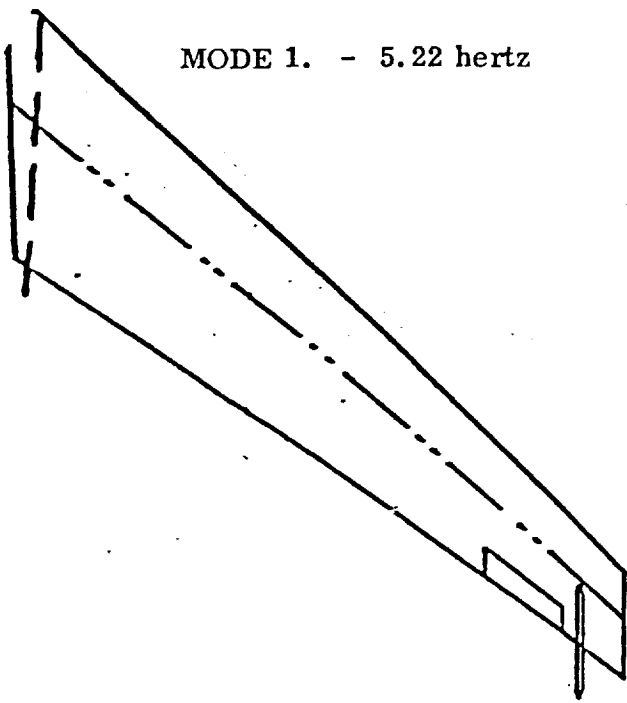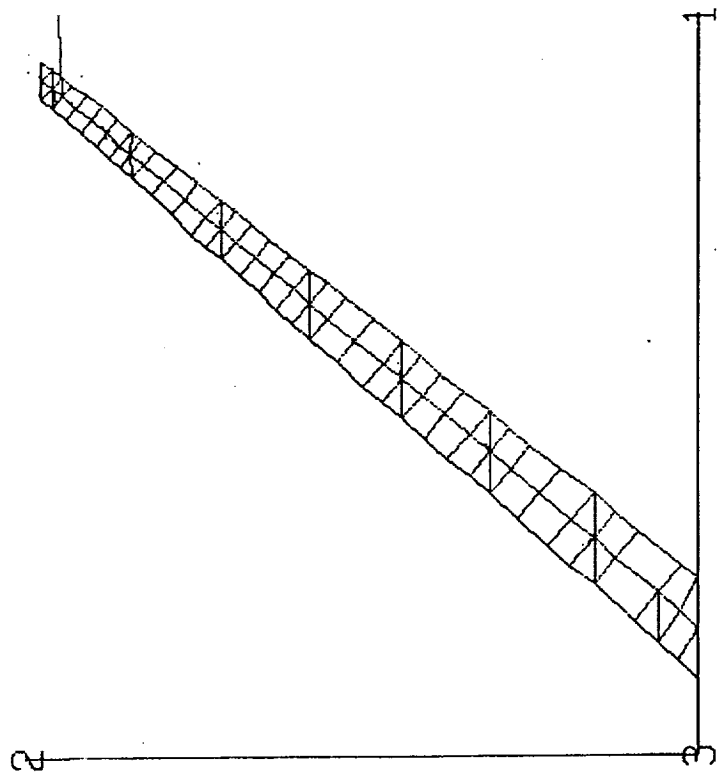
MODE 3. - 26.04 hertz

MODE 4. 45.96 hertz
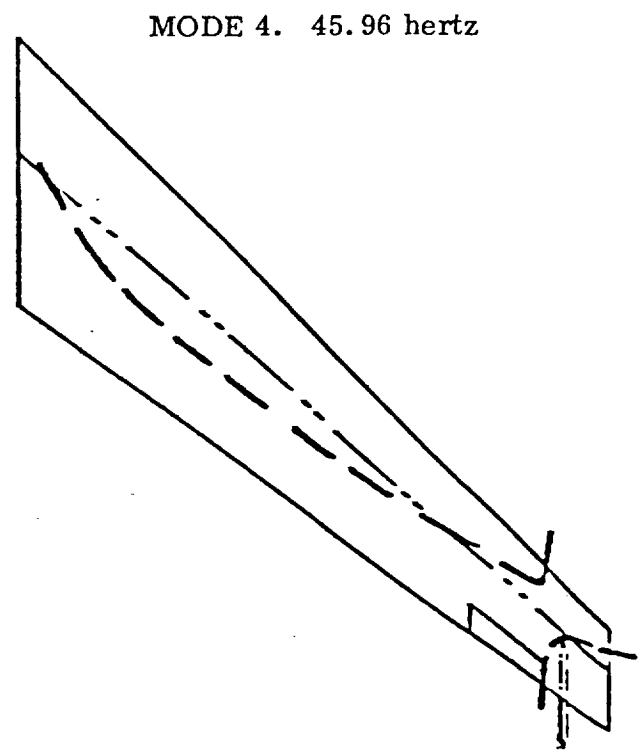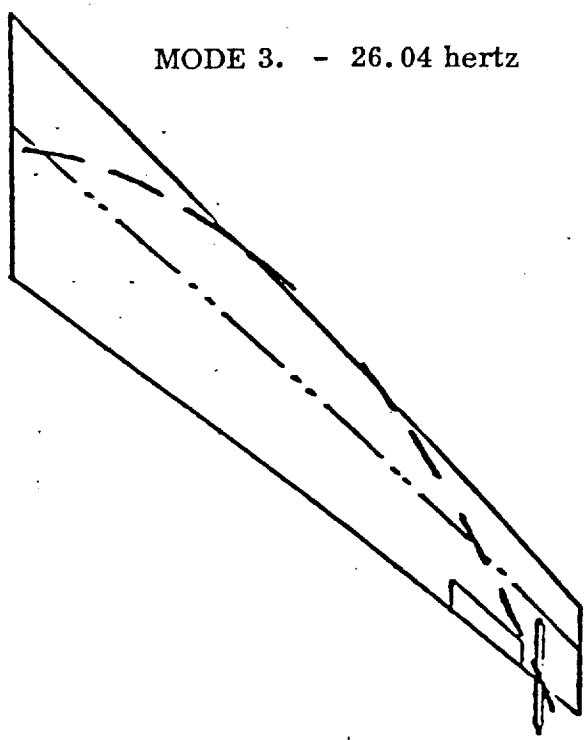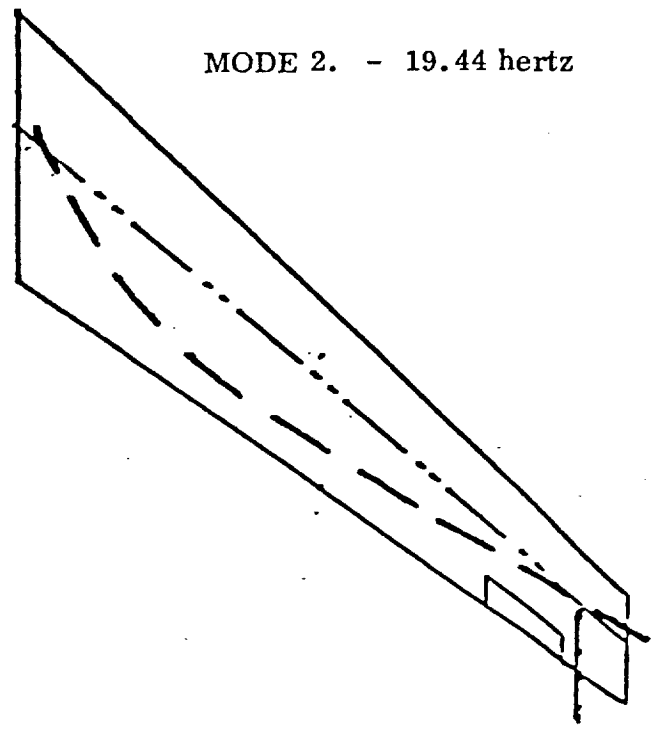
Fig. 8 Measured nodal patterns and frequencies

VIBRATIONAL MODE, FREQ (HZ) .527873 X10 +01 1/1/1.

Fig. 9a Mode 1 (5 Hz)

WIND TUNNEL MODEL

SPEC
1.1

VIBRATIONAL MODE, FREQ (HZ) .189037 X10 +02 1/1/3
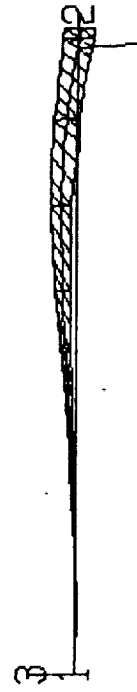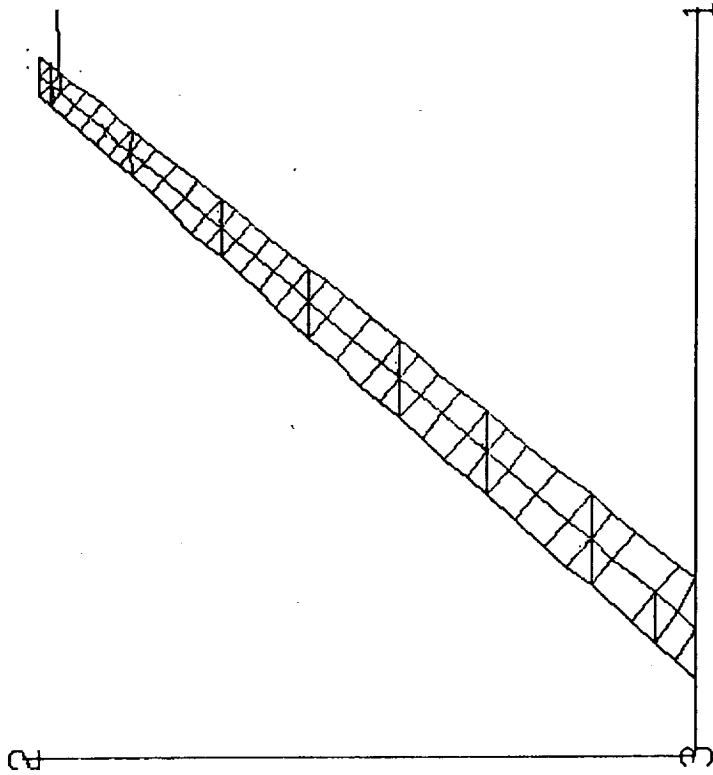
WIND TUNNEL MODEL

SPEC
1.1

Fig. 9b Mode 2 (19 Hz)

-32-

VIBRATIONAL MODE, FREQ (HZ)   .260087 X10 +02   1/1/4

-33-
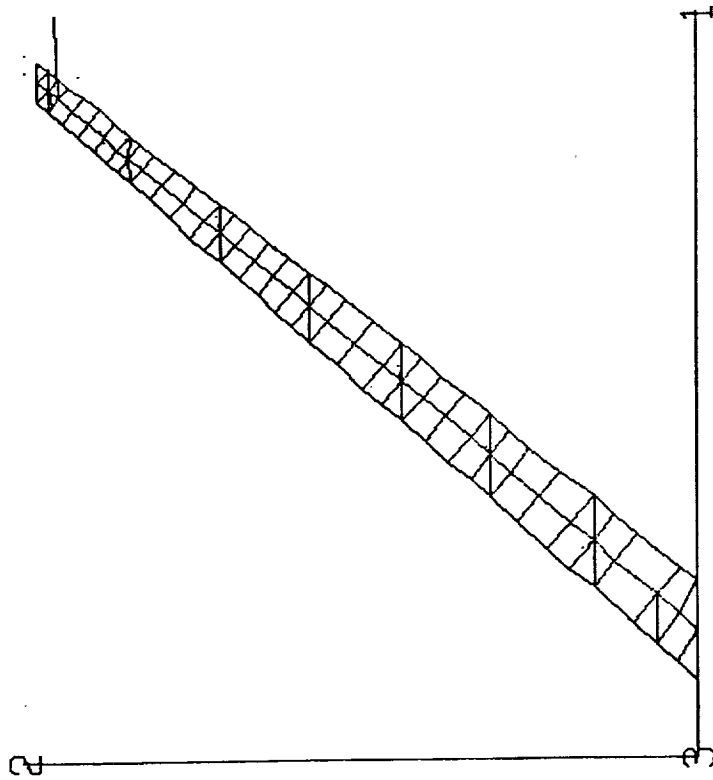
WIND TUNNEL MODEL

SPEC
1.1

Fig. 9c Mode 3 (26 Hz)

VIBRATIONAL MODE, FREQ (HZ)   .443395 X10 +02   1/1/5

WIND TUNNEL MODEL

SPEC
1.1

-34-
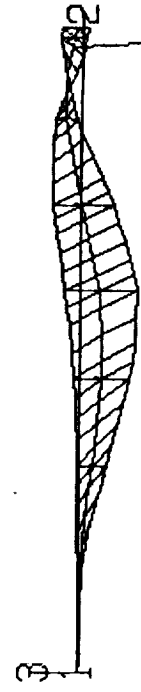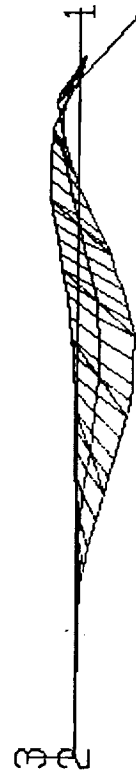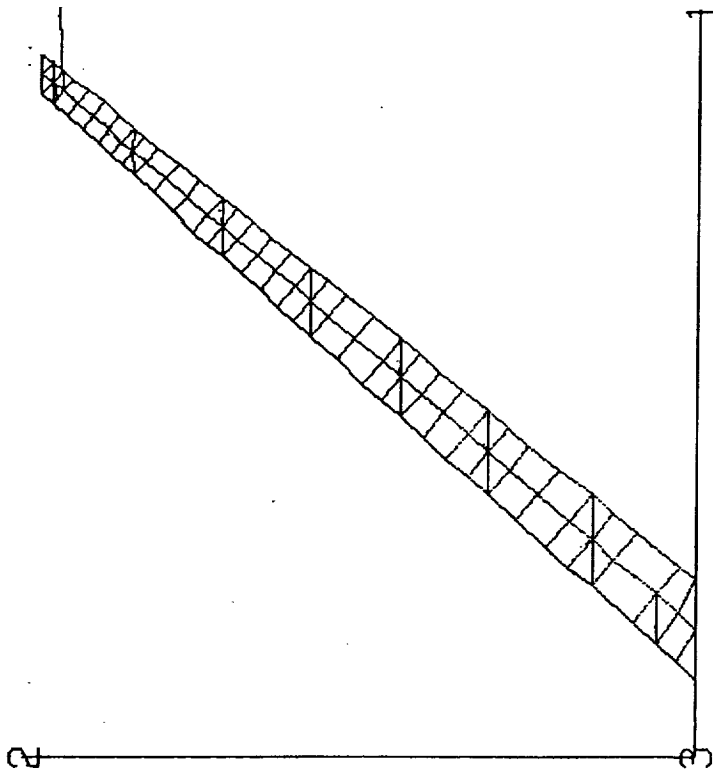
Fig. 9d   Mode 4 (44 Hz)

VIBRATIONAL MODE, FREQ (HZ)   .601990 X10 +02   1/1/7
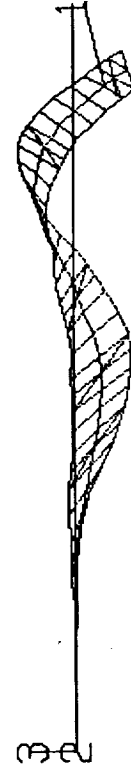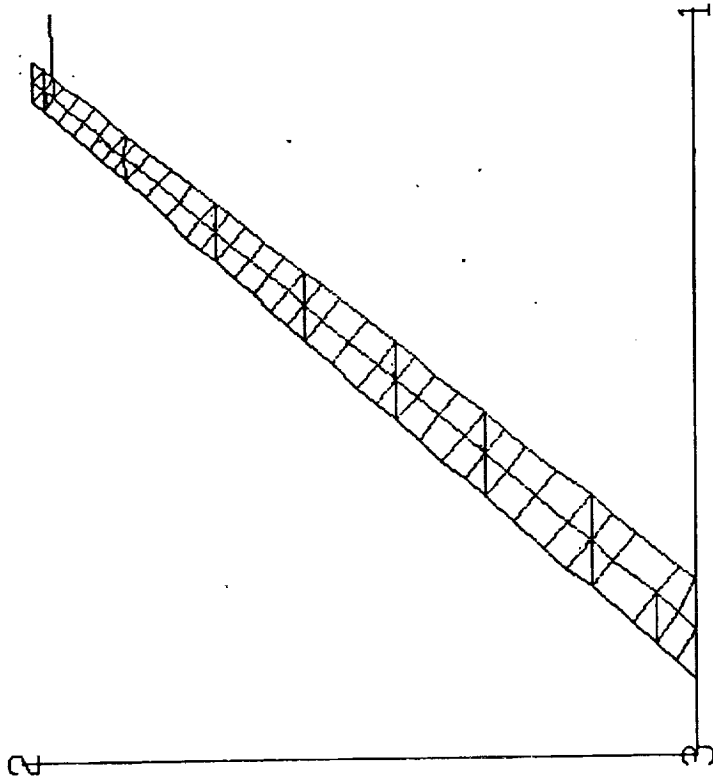
WIND TUNNEL MODEL

SPEC
1.1

Fig. 10 Mode 5 (60 Hz)

VIBRATIONAL MODE, FREQ (HZ) .738675 X10 +02 1/1/8

WIND TUNNEL MODEL

SPEC
1.1

-36-

Fig. 11 Mode 6 (74 Hz)

MODE 1. - 5.456 hertz

(12a)

MODE 2. - 18.535 hertz

(12b)

MODE 3. - 24.880 hertz

(12c)

MODE 4. = 42.129 hertz

(12d)
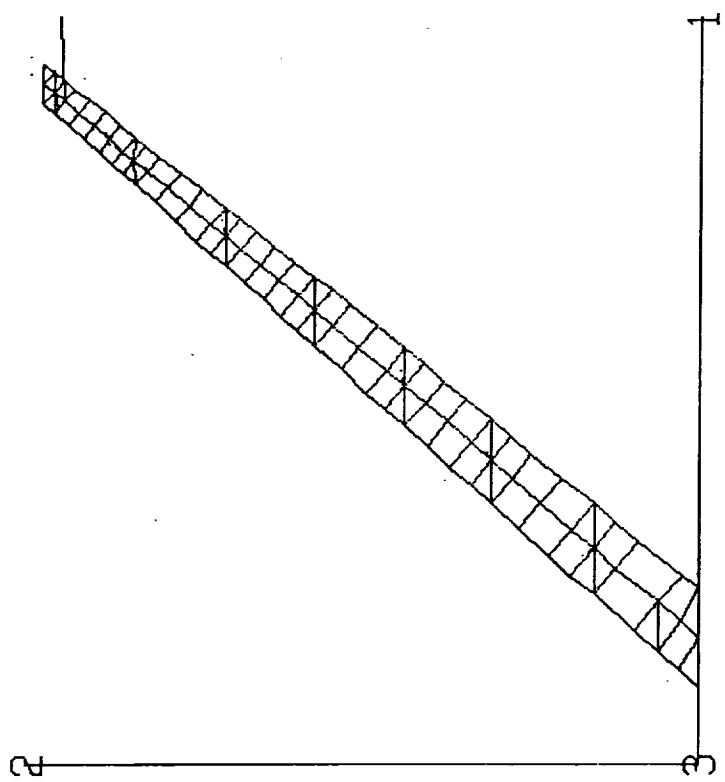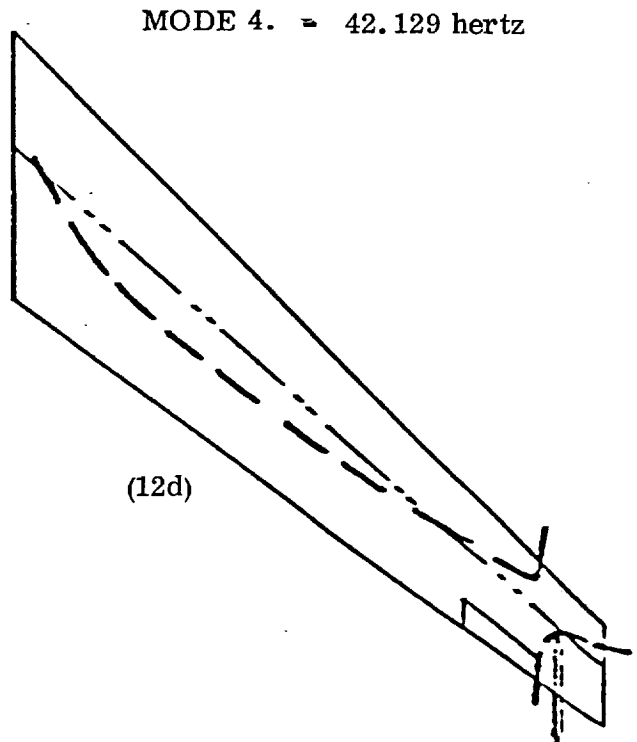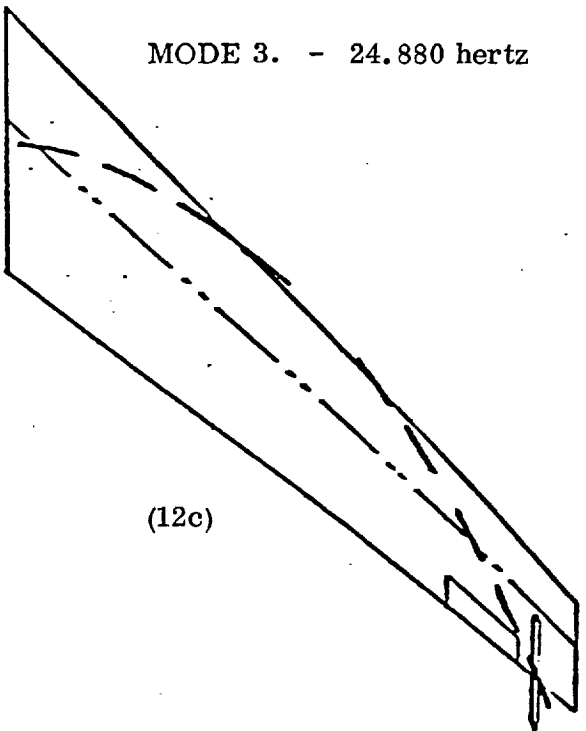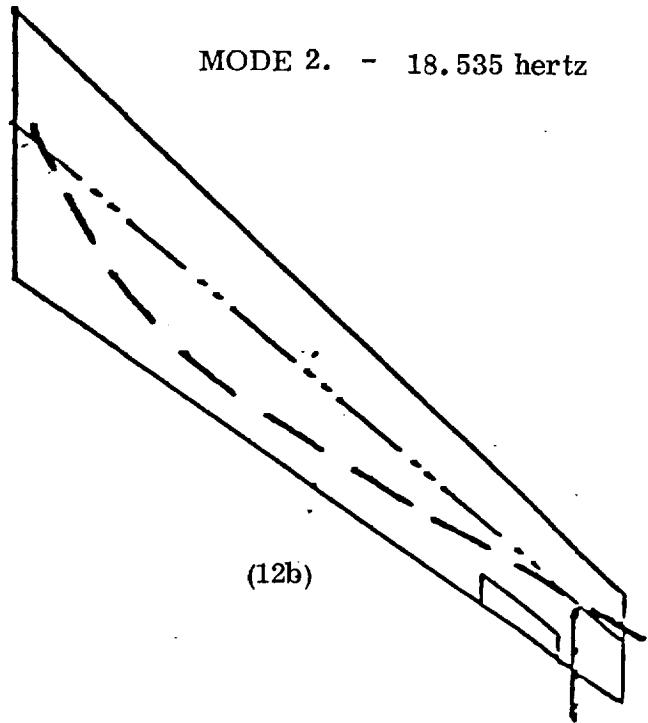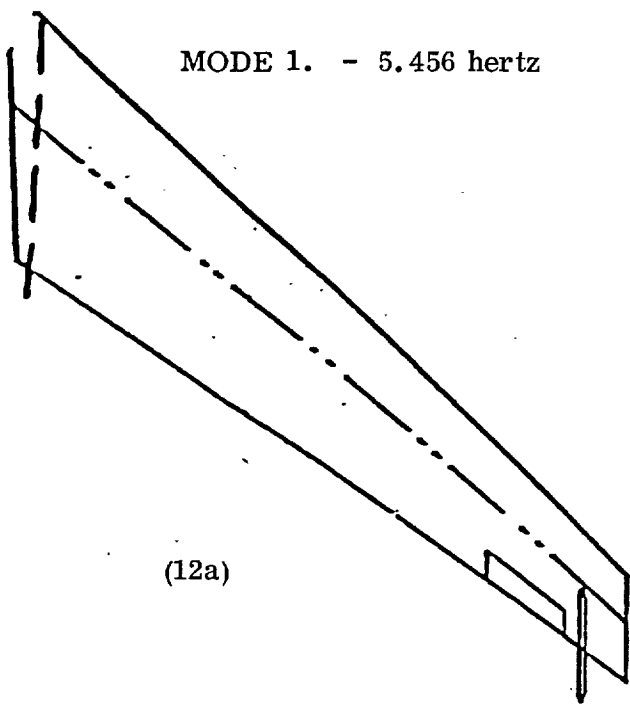
Fig. 12 First Four Normal Modes of Reduced Dynamical System at
Zero Airspeed

TABLE 6

COMPARISON OF VIBRATION MODES

	Vibration Test Freq.	(Hz) SPAR 666 DOF	Reduced Model 15 DOF
1	5.22	5.279	5.456
2	19.44	18.90	18.54
3	26.04	26.01	24.88
4	45.96	44.34	42.13
5	N/A	60.19	61.67
6		73.87	68.42
7		84.96	93.02
8		93.18	105.45
9			126.12
10			135.01
11			146.70
12			204.40
13			297.65
14			420.15
15			894.27

HO

ROW	COL 8	COL 9	COL 10	COL 11	COL 12	COL 13	COL 14	COL 15
1	.47960304329522E+00	.30938836758074E+00	.14379981198948E+00	.62189944115992E-01	.23050522226734E-01	.73474321303967E-02	.29192273863077E-02	.18105768191101E-02
2	.34726914402290E+00	.30707891008031E+00	.20265928559159E+00	.10327093892545E+00	.37424964999275E-01	.10519437366696E-01	.36235591700040E-02	.21762804849787E-02
3	.21852796345223E+00	.23441252645723E+00	.23192529628848E+00	.17377830921430E+00	.79366009230244E-01	.20855418710240E-01	.59165005967364E-02	.33884384941696E-02
4	.15475688801722E+00	.16042793869316E+00	.19793974317559E+00	.21807702222573E+00	.15072155726338E+00	.50839136709652E-01	.12919891373843E-01	.88254667409022E-02
5	.11524769253383E+00	.10935758439665E+00	.13101754364822E+00	.18745115396339E+00	.19977923411428E+00	.11396215494491E+00	.32223911081791E-01	.38531487013011E-01
6	.74166368768255E-01	.67849082552531E-01	.72150230068283E-01	.99711480307608E-01	.13576897512925E+00	.17355091235684E+00	.86096124552568E-01	.10961422423176E+00
7	.38687345082832E-01	.34792293079920E-01	.35568940754557E-01	.45383028152794E-01	.55187801035854E-01	.87812483434681E-01	.12833693867012E+00	.60619467927660E-01
8	-.72132710152415E-01	.26187091142867E-01	-.49696718771303E-03	-.48946165509134E-02	-.21780010422747E-02	-.45065066709607E-03	-.83819283025664E-04	-.26448579398491E-04
9	-.56194821833307E-01	-.42473443811793E-01	-.17290072716715E-01	-.49663422902717E-03	-.26537275400336E-02	-.10776884556034E-03	-.10776884556034E-03	-.28917355289270E-04
10	-.34958589453866E-01	-.36962956827153E-01	-.30558733482899E-01	-.14086690616867E-01	-.73988866636285E-03	-.35520755218040E-03	-.35520755218040E-03	-.12451408931519E-03
11	-.21938675865776E-01	-.23408829273963E-01	-.27577450160630E-01	-.24902093333416E-01	-.11603645330932E-01	-.10686003402009E-02	-.10686003402009E-02	-.87930945670047E-03
12	-.14163595725806E-01	-.13586824830366E-01	-.16581977023579E-01	-.22281032960057E-01	-.21614261011012E-01	-.63354260617785E-02	-.16929944034647E-02	-.51350114400635E-02
13	-.88955021212321E-02	-.81353306853598E-02	-.86620707968684E-02	-.11978186359249E-01	-.17320512925917E-01	-.17699423619434E-01	-.30780362552851E-02	-.12623532027913E-01
14	-.49980025407984E-02	-.44747462597773E-02	-.45492246639708E-02	-.57485259738853E-02	-.70050409488994E-02	-.11593905208153E-01	-.13527359803464E-01	-.25787114750002E-02
15	-.39917195570764E-04	-.35351010418122E-04	-.34525819940951E-04	-.39003746881396E-04	-.61081261373966E-04	-.38561405386762E-03	-.18335770836362E-03	-.11973874465723E-02

TABLE 7b – H1

H1

ROW	COL 1	COL 2	COL 3	COL 4	COL 5
1	0.	0.	0.	0.	0.
2	0.	0.	0.	0.	0.
3	0.	0.	0.	0.	0.
4	0.	0.	0.	0.	0.
5	0.	0.	0.	0.	0.
6	0.	0.	0.	0.	0.
7	0.	0.	0.	0.	0.
8	0.	0.	0.	0.	0.
9	0.	0.	0.	0.	0.
10	0.	0.	0.	0.	0.
11	0.	0.	0.	0.	0.
12	0.	0.	0.	0.	0.
13	0.	0.	0.	0.	0.
14	0.	0.	0.	0.	0.
15	0.	0.	0.	0.	0.

ROW	COL 6	COL 7	COL 8	COL 9	COL 10
1	0.	-.17757257247995E+02	.36946818527441E+03	-.23834118718183E+03	-.11077797841650E+03
2	0.	-.32129552744959E+02	-.29813260426005E+03	-.26362905184987E+03	-.17398418958512E+03
3	0.	-.75359169878111E+02	-.20749545127601E+03	-.22257807281780E+03	-.22021641192049E+03
4	0.	-.16086973228054E+02	.16517676433162E+03	-.17122965033292E+03	-.21068438513361E+03
5	0.	-.24207673677975E+03	-.13964807430394E+03	-.13251090530088E+03	-.15875676172971E+03
6	0.	-.19086252941611E+03	-.10426226409441E+03	-.95381492732116E+02	-.10142799852295E+03
7	0.	-.90651251786810E+02	-.63547671663822E+02	-.57149675490549E+02	-.58425393721430E+02
8	0.	-.16778505409382E+01	.55568332794078E+02	.20173552227013E+02	-.38284487046601E+00
9	0.	-.22782407136545E+01	.48243585321198E+02	.36463701522267E+02	.14843629201105E+02
10	0.	-.70253495385947E+00	.33193940484249E+02	.35096860311072E+02	.29015957931741E+02
11	0.	-.12384925897482E+02	.23415820385574E+02	.24984960124509E+02	.29342568166573E+02
12	0.	.26190458663327E+02	.17162329456237E+02	.16464344924509E+02	.20092733865588E+02
13	0.	.24348986244285E+02	.12505198876785E+02	.11436558247348E+02	.12177043678738E+02
14	0.	.11506451043868E+02	.81962288404962E+01	.73501995408232E+01	.74725374577186E+01
15	0.	-.14802692078936E+00	-.96737025627442E-01	-.85671138763163E-01	-.83671337143775E-01

ROW	COL 11	COL 12	COL 13	COL 14	COL 15
1	-.47908798987113E+02		-.56601859675151E+01	-.22488632211613E+01	-.13948004313290E+01
2	-.88658708947388E+02		-.90309988994499E+01	-.31108269138176E+01	-.18683496064998E+01
3	-.16505005093190E+03		-.19802520686492E+02	-.56178026001852E+01	-.32130085540345E+01
4	-.23276028206496E+03		-.54262167007384E+02	-.13789795594805E+02	-.94196903670960E+01
5	-.22713854049104E+03		-.13809036113163E+03	-.39046396766598E+02	-.46689414294458E+02
6	-.14017330045606E+03		-.24397596051226E+03	-.12103298334129E+03	-.15409446876270E+03
7	-.74545972745821E+02		-.14424041901407E+03	-.21080572015223E+03	-.99573285167224E+02
8	-.37706288981228E+01		-.34716436121968E+00	-.64571229943974E-01	-.20374992965725E-01
9	-.42636340893757E+00		-.64629424008446E+00	-.92520188268885E-01	-.24825719730903E-01
10	-.13375515793765E+00		-.14629424008336E+00	-.33727469094559E+00	-.11822797261705E+00
11	.26578708935435E+02		-.90235196661627E+00	-.11405498573913E+01	-.93851390252737E+00
12	.26998400384204E+02		.76767701805663E+01	-.20514372396962E+01	-.62222023137119E+01
13	.16838802415513E+02		.24881654722560E+02	-.43270694557486E+01	-.17746022246379E+02
14	.94425047869692E+01		.19044100335482E+02	-.22219984789121E+02	-.42357807127545E+01
15	-.94523353116552E-01		-.93451346162797E+00	-.44356851211000E+00	-.29031355928284E+01

TABLE 7c – H2

H2

ROW	COL 1	COL 2	COL 3	COL 4	COL 5	COL 6	COL 7	COL 8	COL 9	COL 10	COL 11	COL 12	COL 13	COL 14	COL 15
1	.17967525635362E+01	.11592308388108E+01	.47825725198244E+00	-.14451511879646E+00	-.14416670626520E-01	.12886357663555E-01	.88738387801508E-02	.80456846198243E+00	-.45514537720549E-01	.48443944481466E+00	.40664987138056E+00	.19105179897757E+00	.48806668766144E+00	.58419925528044E-02	-.15129402983004E-02
2	-.13921596715400E+01	-.12595516830938E+01	-.81038650836111E+00	-.37586803578084E+00	-.98912546292216E-01	.35899022233308E-02	.66159402866350E-02	-.42341061933126E+00	-.41512155600361E+00	.54591313192510E-01	-.33293367616422E+00	.23618450093134E+00	.84134568820848E+00	.21458478167381E-01	-.77729510186475E-02
3	-.91399970483158E+00	-.10305044971690E+01	-.10305065811112E+01	-.78031911465710E+00	-.34415737779586E+00	-.61640828309664E-01	-.49022133394958E-02	-.17253178612219E+00	-.19897082076272E+00	.38688626781688E+00	-.47534898998076E-01	.19146147478790E+00	.12972998585241E+01	.48167379846340E+00	.25730916795870E-01
4	-.68094518015924E+00	-.74402113067460E+00	-.95883317600004E+00	-.11074784830320E+01	-.80042028871934E+00	-.24424279211364E+00	-.46559727373374E-01	-.48662202877278E+00	.22543294563385E+00	.25346462351164E+00	.43589599147014E+00	-.13419954192725E+00	.13701496065598E+00	.86732415059984E-01	.59807497148250E-01
5	.53960838381638E+00	.53727866316722E+00	.68739289052238E+00	-.10563098705663E+01	-.12141938022883E+01	-.68424341120818E+00	-.18210091585307E+00	-.60467936526272E+00	.42678329674041E+00	.11332244181079E+00	-.35811372613047E+00	-.55233872670678E+00	.76941268230058E+00	.11224347439131E+00	.98004658851590E-01
6	-.37301653715568E+00	-.35754783634562E+00	-.40787664698066E+00	-.62130727462706E+00	-.93696392884230E+00	-.12254405813752E+01	-.62132879786316E+00	.60173381477280E+00	.46440494621986E+00	.27862802075639E+00	-.53668512709792E-01	-.29974325521229E+00	.55710832257209E+00	.37723105532122E-01	.14425913284116E+00
7	-.21984688171379E+00	-.20610670534228E+00	-.22573283405666E+00	-.31925578308482E+00	-.43386390438802E+00	-.71143918153331E+00	-.10873220260018E+01	.41224804274743E+00	.32712446838717E+00	.22182009434731E+00	-.12310433810373E+00	-.12867065793365E+00	.28005258502855E+00	.61448825591006E-01	-.18881984562278E-01
8	.16644899744813E+00	.42737303767931E-01	.24292422232090E+00	-.27674007103230E-01	-.11505386232278E-01	-.17716939483881E-02	-.24838728893281E-03	.34454791936749E+00	-.22851657152439E+00	-.71603262695075E-01	-.41467679935694E-04	.16489588735586E-01	.10387129389973E+00	.45976537458710E-01	-.24201513055991E-02
9	-.14271917244366E+00	-.10536986051276E+00	-.32169712170705E-01	-.14327894585377E-01	-.17090611845611E-01	-.48653238413909E-02	-.89365499193160E-03	-.20508017467236E+00	-.20763219640909E+00	-.12964159044224E+00	-.47326981653291E-01	-.12211679010042E-01	.79356777426932E-02	.47129850048339E-02	-.29986189177892E-02
10	-.92031393393205E-01	.10260004522277E+00	.84131501390853E-01	-.32678441170793E-01	-.77468240540620E-02	-.95758270544349E-02	-.28129447433326E-02	-.10406574299916E+00	-.12783146470405E+00	-.14039495314170E+00	-.99534711463005E-01	-.34079686817715E-01	.51724148514850E-01	.38642791744669E-02	-.32895912449416E-02
11	.58847550126793E-01	.68263392718748E-01	.86003508091349E-01	.79522893739700E-01	.34776803990511E-01	.85827028128826E-02	-.65554986867825E-02	-.77754475497687E-01	-.74495193042118E-01	.95061300548953E-01	-.11143176528322E+00	-.72322129258371E-01	-.17409991350228E+00	.82300878635749E-03	-.36154943245626E-02
12	-.38750329772411E-01	.40458108414911E-01	.55336473879347E-01	.81342149655375E-01	.84507606399288E-01	.21375724295434E-01	-.10334776923243E-01	-.67200687847829E-01	.54791607431133E-01	-.49415974560181E-01	-.71297705914999E-01	-.83422532165989E-01	.51121546448939E+00	.90770167669746E-02	-.15821969084747E-02
13	.25383583144474E-01	.25146000808543E-01	.30245974267221E-01	-.47881273820422E-01	.78211742075557E-01	.81368895016390E-01	-.12167576541185E-01	.57308867404652E-01	.45258112460181E-01	-.33458112460651E-01	-.29484832183034E-01	-.38416390295813E-01	-.65582412566628E-01	.36038715963542E-01	-.31875094556259E-01
14	-.15508347599114E-01	-.19440583574450E-01	-.17192828251629E-01	-.25206622879750E-01	.35368864728322E-01	.61703664903649E-01	-.75062512975319E-01	.42156789751411E-01	-.33690762202517E-01	.25090736070728E-01	-.19963374323330E-01	-.14348883261662E-01	.18560685162800E+00	.45405984241306E-01	-.24163133896156E-01
15	-.55530489554347E-02	-.47638968337486E-03	-.42995487166015E-03	-.46349010012633E-01	-.70529778973708E-03	-.47393785068563E-02	-.23884928500915E-02	-.72141153828264E-04	.25734918520653E-04	-.18368049770217E-01	-.65421515519192E-02	-.26062284741294E-02	-.84406622383531E-02	-.34923102594844E-02	-.64508391536222E-02

-41-

H3

ROW	COL 1	COL 2	COL 3	COL 4	COL 5
1	-.77731977499158E-02	-.64095953897748E-02	-.53601360290080E-02	-.47796267028814E-02	-.41795808068156E-02
2	0.	0.	0.	0.	0.
3	0.	0.	0.	0.	0.
4	0.	0.	0.	0.	0.
5	0.	0.	0.	0.	0.
6	0.	0.	0.	0.	0.
7	0.	0.	0.	0.	0.
8	-.46424703050472E-03	-.34502618343335E-03	-.25940533344378E-03	-.20631200071066E-03	-.15860833895172E-03
9	0.	0.	0.	0.	0.
10	0.	0.	0.	0.	0.
11	0.	0.	0.	0.	0.
12	0.	0.	0.	0.	0.
13	0.	0.	0.	0.	0.
14	0.	0.	0.	0.	0.
15	0.	0.	0.	0.	0.

ROW	COL 6	COL 7	COL 8	COL 9	COL 10
1	-.26170329005440E-02	-.35266568794890E-02	-.46424703050472E-03	-.34502618343335E-03	-.25940533344378E-03
2	0.	0.	0.	0.	0.
3	0.	0.	0.	0.	0.
4	0.	0.	0.	0.	0.
5	0.	0.	0.	0.	0.
6	-.87590869812748E-04	-.10150293705114E-03	-.13126479458484E-02	-.87929545786596E-03	-.59438958336294E-03
7	-.13294527134763E-04	0.	0.	0.	0.
8	0.	0.	0.	0.	0.
9	0.	0.	0.	0.	0.
10	0.	0.	0.	0.	0.
11	0.	0.	0.	0.	0.
12	0.	0.	0.	0.	0.
13	0.	0.	0.	0.	0.
14	0.	0.	0.	0.	0.
15	0.	0.	0.	0.	0.

ROW	COL 11	COL 12	COL 13	COL 14	COL 15
1	-.20631200071066E-03	-.15860833895172E-03	-.87590869812748E-04	-.10150293705114E-03	-.46639450285300E-04
2	0.	0.	0.	0.	0.
3	0.	0.	0.	0.	0.
4	0.	0.	0.	0.	0.
5	0.	0.	0.	0.	0.
6	0.	0.	0.	0.	0.
7	0.	0.	0.	0.	0.
8	0.	0.	0.	0.	0.
9	0.	0.	0.	0.	0.
10	0.	0.	0.	0.	0.
11	-.42174771214406E-03	-.28514618786854E-03	-.13880831572294E-03	-.10150293705114E-03	-.52881157745323E-05
12	0.	0.	0.	0.	0.
13	0.	0.	-.56284900123975E-05	0.	-.13867147673813E-05
14	0.	0.	0.	0.	0.
15	0.	0.	0.	0.	0.

TABLE 8 – Damping Matrix

DAMPING MATRIX

ROW	COL 1	COL 2	COL 3	COL 4	COL 5
1	-.94182356438886E+02	.19460999612155E+02	-.35883762035238E+01	.33990616015140E+00	-.10574113186904E+00
2	.19460999612155E+02	-.36039236483565E+02	.17111816361562E+02	-.23109176962964E+01	.28949742177018E+00
3	-.35883762035238E+01	.17111816361562E+02	-.28449051185437E+02	.13314819060728E+02	-.17191775020049E+01
4	.33990616015490E+00	-.23109176962964E+01	.13314819060728E+02	-.21376334742799E+02	-.10433495009717E+02
5	-.10574113186729E+00	.28949742177018E+00	-.17191775020049E+01	.10433495009717E+02	-.16300436020384E+02
6	.70808753774555E-02	-.87655819690311E-01	.21067994760517E+00	-.11931366110757E+01	.79314717167627E+01
7	-.63990734173442E-01	-.15201805706703E-01	-.83720018039283E-01	.31637492350090E+00	-.10163711883155E+01
8	.81235002428473E+00	.24512959261635E+00	-.45397377651300E-01	-.20349558335036E-02	-.34212300098002E-02
9	.28072905219609E+00	.11419422541985E+00	.19058334764783E+00	-.48574387321832E-01	-.83233209980171E-03
10	-.61299438532614E-01	.20941351143317E-01	.14648448431036E+00	.10417936529582E+00	-.44554591156956E-01
11	-.12915926283505E-02	-.47730206973700E-01	-.13583774949554E+00	.73667631323449E-01	-.12264036744299E+00
12	.25580506478785E-02	.17094091756535E-01	.33172527950358E-01	-.14835468495214E+00	.11333990102024E+00
13	.19690802173471E-04	.28134384814336E-02	.56477932966438E-02	.34989094249404E-01	-.16792341613761E+00
14	-.31105421785015E-03	-.44632041868224E-03	-.14843324408772E-02	-.31517573414548E-02	.10820547088647E-01
15	.96228974957141E-04	-.34234754398329E-02	.13358422639331E-02	-.52953072847640E-02	.23542994371870E-01

ROW	COL 6	COL 7	COL 8	COL 9	COL 10
1	-.70808753766149E-02	-.63990734193407E-02	.81235002428473E+00	-.28072905219609E+00	.61299438532170E-01
2	-.87656819690836E-01	-.15201805705547E-01	.24512959261635E+00	.11419422541985E+00	-.20941351143317E-01
3	.21067994760517E+00	.83720018036831E-01	-.45397377651745E-01	.19058334764827E+00	.14648448443103E+00
4	-.11931366110757E+01	.31637492348339E-01	-.20349558332412E-02	-.48574387321832E-01	.10417936529582E+00
5	.79314717167627E+01	-.10163711883155E+01	-.34221300097781E-02	-.83293209561005E-03	-.44554591156956E-01
6	-.11844537745344E+02	.46935696019965E+01	-.10246380519927E-02	-.32969652157764E-02	-.19381445720865E-01
7	.46935696019965E+01	-.37404589954459E+01	-.14158136161998E-02	-.36263544558927E-02	-.12416480709438E+00
8	-.10246380521062E-02	-.14158136169980E-02	.77714685111268E+00	.90313063948790E-01	-.89428634255559E-01
9	-.32969652157409E-02	-.36263544552967E-02	.90313063948677E-01	.34332593517315E+00	.89428634255677E-01
10	-.19381445724423E-01	-.62433633430778E-02	-.12416480709436E+00	.89428634255677E-01	.25008826852286E+00
11	-.29998998506399E-01	.87165585018484E-01	.33889341974249E-01	-.14315106036283E-01	.63338765143983E-01
12	.39643580087034E-01	.32608233732986E-01	.11484516458461E-02	.37734101525165E-02	.99439733398772E-02
13	.16121036133065E+00	.18236688103803E-01	.55587346688438E-03	.17896780016945E-02	.33196519252772E-02
14	-.15466021492124E+00	.15954584851031E+00	.48530445190608E-03	.14493696948606E-02	.24825285340093E-02
15	.38984304491420E+00	-.23224996184346E-01	.80639833822808E-05	.17573926141750E-04	.64987310582011E-04

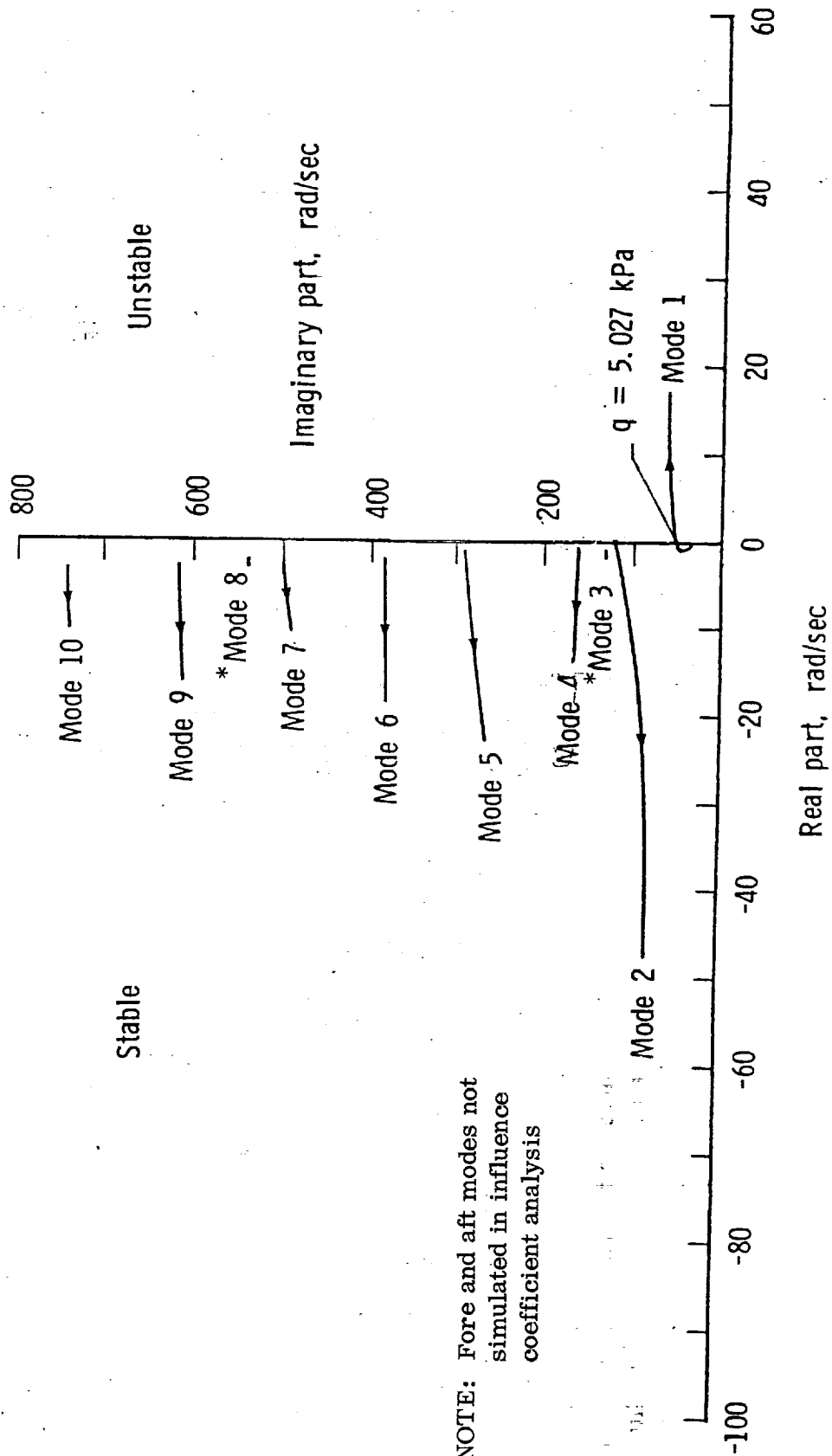| ROW	COL 11	COL 12	COL 13	COL 14	COL 15
1	-.12915926283594E-02	.25580506478741E-02	.19690802153854E-04	.31105421784970E-03	.96228974975823E-04
2	-.47730206973700E-01	.17094091756135E-01	.28134384813268E-02	.44632041866000E-03	-.34234754394726E-03
3	-.13583774949554E+00	.33172527950403E-01	-.56477932967328E-02	.14843324399920E-02	-.13358422639054E-02
4	-.73667631322115E-01	-.14835468495214E+00	.34989094249404E-01	-.31517573414503E-02	-.52953072848085E-02
5	-.12264036746209E+00	.11333990102024E+00	-.16792341613761E+00	-.10820542088647E-01	.23542994371870E-01
6	-.29998998506487E-01	.39643580086990E-01	.16121036133065E+00	.15466021492124E+00	.38984304491420E+00
7	.87165585017150E-01	.32608233732986E-01	.18236688103758E-01	.15954584851031E+00	.23224996184346E-01
8	-.33389341974475E-02	-.11484516458687E-02	.55587346688103E-03	.48530445191964E-03	.80639833877154E-05
9	.14315106036283E-01	.37734101525165E-02	.17896780016832E-02	.14493696948433E-02	.17573932613159E-04
10	.63338765143983E-01	.99439733398884E-02	.33196519252885E-02	.24825285341106E-02	.64987310582453E-04
11	-.18036682787388E+00	-.45519540940867E-01	.89434788864816E-02	.45005523792804E-02	.10114749254785E-01
12	-.45519540940867E-01	-.12586937404409E+00	.32724779922164E-01	.84187963724257E-01	.69139850857321E-03
13	.89434788864816E-02	.32724779922164E-01	-.11768374107141E-01	-.32862793811107E-01	.14127391087648E-01
14	.45005523792804E-02	.84187963724257E-01	-.32862793811107E-01	.83066369281639E-01	.39553551967730E-01
15	.10114749254570E-01	.69139850857321E-03	.14127391087648E-01	.39553551967730E-01	-.14551771692813E-01
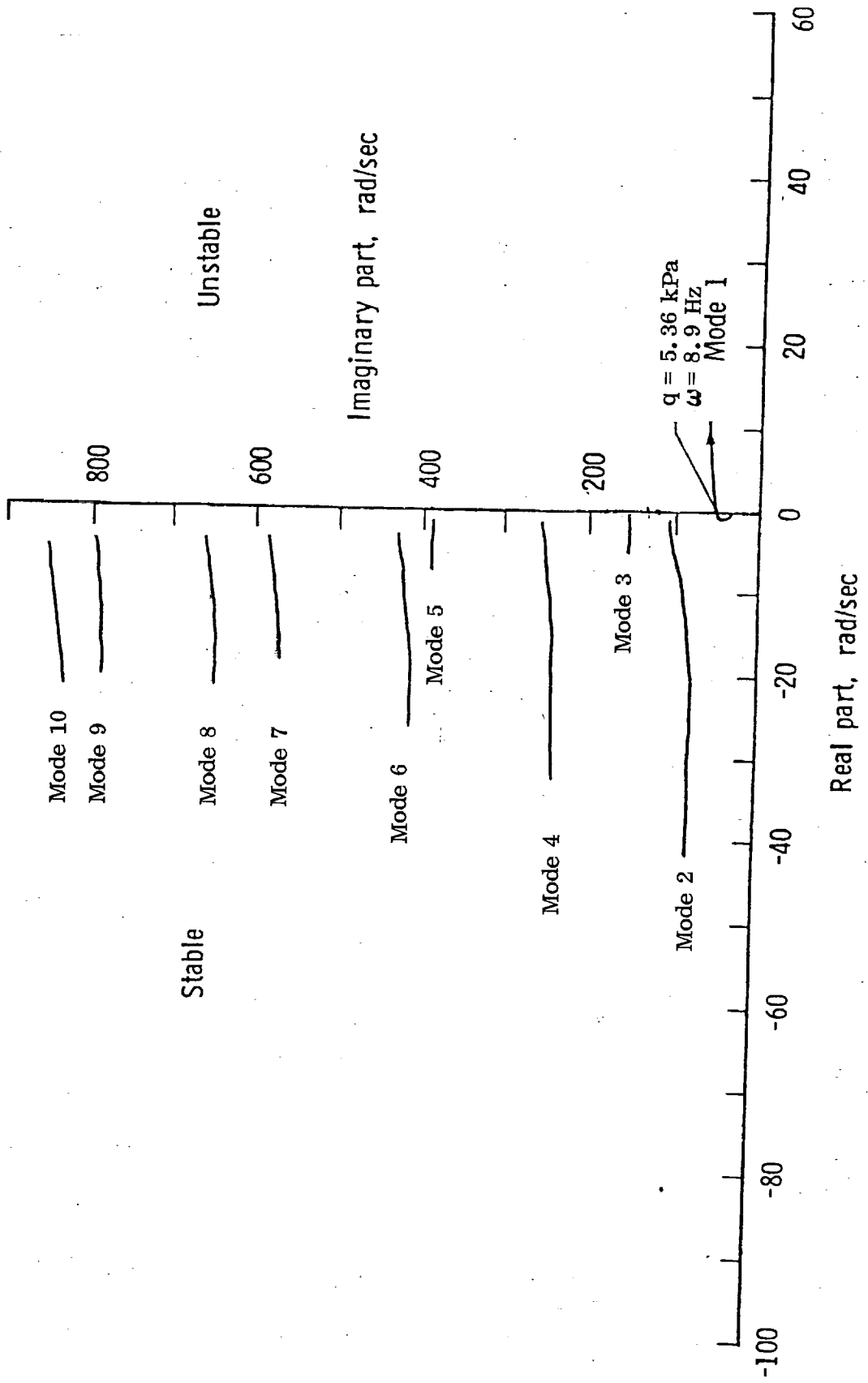
Fig. 13.   Open Loop Flutter Analysis of the DAST wing for fixed
Mach Number = .897 and v = 136. m/sec

Unstable

Imaginary part, rad/sec

Mode 1

q = 5.027 kPa

800

600

*Mode 8

400

Mode 10

Mode 9

Mode 7

200

Mode 6

Mode 5

Mode 4

*Mode 3

Mode 2

Real part, rad/sec

-100   -80   -60   -40   -20   0   20   40   60

Stable

*NOTE: Fore and aft modes not simulated in influence coefficient analysis

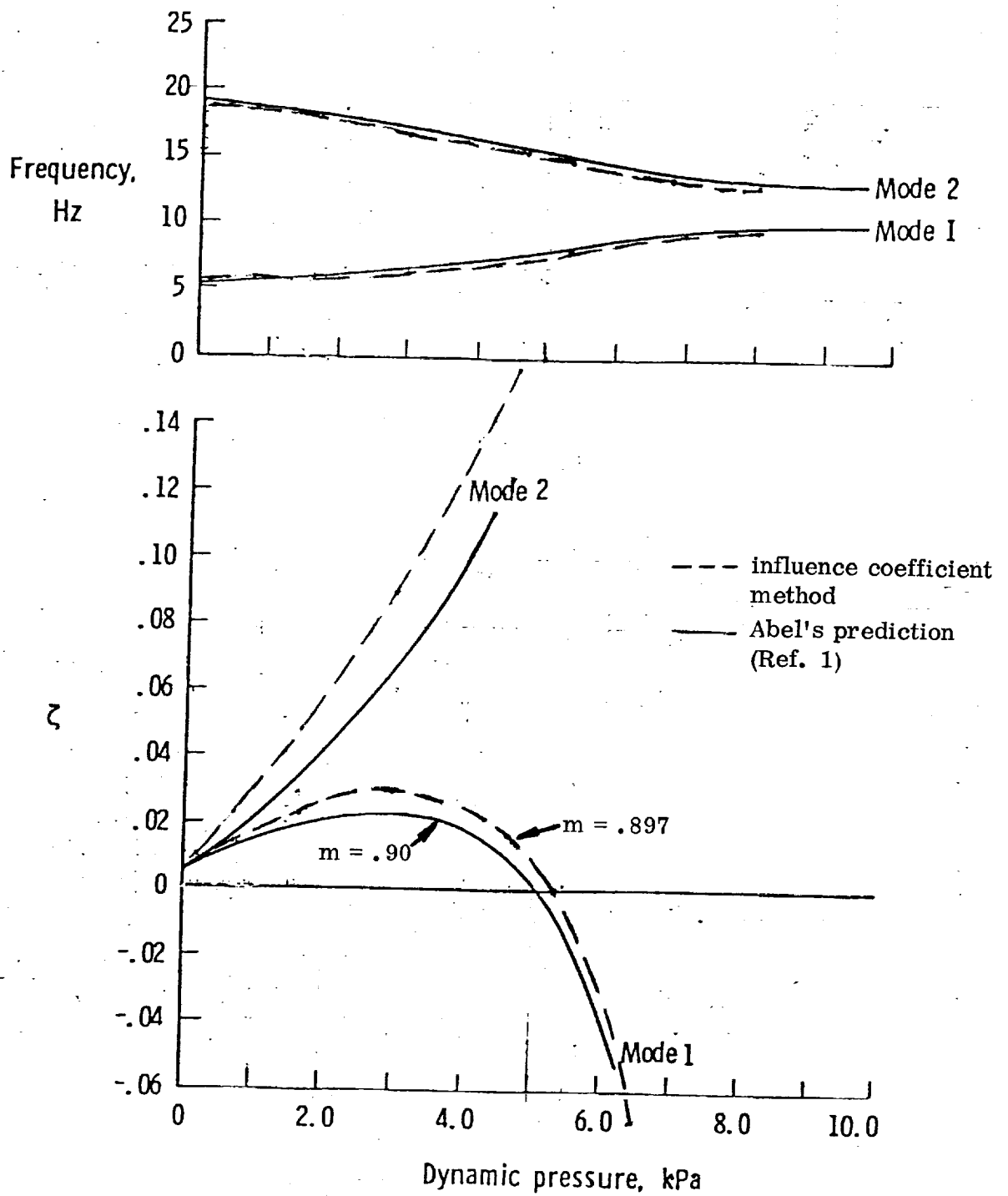Figure 14. Dynamic-pressure root locus at M = 0.90 (system off). Arrows indicate increasing dynamic pressure.

Figure 15. Damping and frequency versus dynamic pressure (system off).

1. Report No. NASA CR 165772	2. Government Accession No.	3. Recipient's Catalog No.
4. Title and Subtitle Final Report An Influence Coefficient Method for the Application of the Modal Technique to Wing Flutter Suppression of the DAST ARW-1 Wing		5. Report Date November 1981
		6. Performing Organization Code
7. Author(s) Samuel Pines Judy McConnell		8. Performing Organization Report No. AMA Report No. 81-25
		10. Work Unit No.
9. Performing Organization Name and Address Analytical Mechanics Associates, Inc. 17 Research Road Hampton, Virginia 23666		
		11. Contract or Grant No. NAS1-15593
12. Sponsoring Agency Name and Address National Aeronautics and Space Administration Washington, D. C. 20546		13. Type of Report and Period Covered Contractor Report
		14. Sponsoring Agency Code

15. Supplementary Notes

Langley Technical Monitor: Aaron J. Ostroff
Final Report

16. Abstract

This report describes the methods used to compute the mass, structural stiffness and aerodynamic forces in the form of influence coefficient matrices as applied to a flutter analysis of the DAST ARW-1 wing. The DAST wing was chosen since wind tunnel flutter test data and zero speed vibration data of the modes and frequencies exist and are available for comparison. The report also contains a derivation of the equations of motion that can be used to apply the modal method for flutter suppression. A comparison of the open loop flutter prediction with both wind tunnel data and other analytical methods is presented.

17. Key Words (Suggested by Author(s)) Flutter Suppression, Pade' Approximants, Unsteady Aerodynamic Influence Coefficients	18. Distribution Statement Unclassified – Unlimited		
19. Security Classif. (of this report) Unclassified	20. Security Classif. (of this page) Unclassified	21. No. of Pages 46	22. Price